NAVAL POSTGRADUATE SCHOOL
Monterey, California

THESIS

MODIFICATION AND VERIFICATION OF DESIGN SIMULATION FOR THERMOACOUSTIC RESEACH SOFTWARE

by

Scott Brian Curtis

March 2000

Advisor:	Thomas J. Hofler
Second Reader:	James V. Sanders

Approved for public release; distribution is unlimited.

20000630 073

REPORT DOCUMENTATION PAGE

Form Approved
OMB No. 0704-0188

Public reporting burden for this collection of information is estimated to average 1 hour per response, including the time for reviewing instruction, searching existing data sources, gathering and maintaining the data needed, and completing and reviewing the collection of information. Send comments regarding this burden estimate or any other aspect of this collection of information, including suggestions for reducing this burden, to Washington headquarters Services, Directorate for Information Operations and Reports, 1215 Jefferson Davis Highway, Suite 1204, Arlington, VA 22202-4302, and to the Office of Management and Budget, Paperwork Reduction Project (0704-0188) Washington DC 20503.

1. AGENCY USE ONLY *(Leave blank)*	2. REPORT DATE March 2000	3. REPORT TYPE AND DATES COVERED Master's Thesis

4. TITLE AND SUBTITLE **Modification and Verification of Design Simulation for Thermoacoustic Research Software**	5. FUNDING NUMBERS
6. AUTHOR(S) Curtis, Scott B.	

7. PERFORMING ORGANIZATION NAME(S) AND ADDRESS(ES) Naval Postgraduate School Monterey, CA 93943-5000	8. PERFORMING ORGANIZATION REPORT NUMBER

9. SPONSORING / MONITORING AGENCY NAME(S) AND ADDRESS(ES)	10. SPONSORING / MONITORING AGENCY REPORT NUMBER

11. SUPPLEMENTARY NOTES

The views expressed in this thesis are those of the author and do not reflect the official policy or position of the Department of Defense or the U.S. Government.

12a. DISTRIBUTION / AVAILABILITY STATEMENT Approved for public release; distribution unlimited.	12b. DISTRIBUTION CODE

13. ABSTRACT *(maximum 200 words)*

This thesis attempts to improve, prepare for release, and verify the accuracy of the expert system code entitled "Design Simulation for Thermoacoustic Research" (DSTAR) created previously by LT Eric Purdy. DSTAR allows a unique new approach for the rapid design and simulation of thermoacoustic devices utilizing a Microsoft Windows™ compliant interface to construct any given thermoacoustic model at runtime. The approach to simulation involves the solution of a one-dimensional acoustic wave equation simultaneously with an energy flow equation from one end of the specified device to the other, including additional lumped elements. The resulting solution is available as both a graphical and text-based output. In order to prepare for release, significant additions to the engine code and interface were completed. Additionally, theoretical results obtained by the DSTAR system code were compared to actual measured values in order to demonstrate potential engineering design applicability.

14. SUBJECT TERMS thermoacoustic simulation, numerical model	15. NUMBER OF PAGES 96
	16. PRICE CODE

17. SECURITY CLASSIFICATION OF REPORT Unclassified	18. SECURITY CLASSIFICATION OF THIS PAGE Unclassified	19. SECURITY CLASSIFI- CATION OF ABSTRACT Unclassified	20. LIMITATION OF ABSTRACT UL

NSN 7540-01-280-5500

Standard Form 298 (Rev. 2-89)
Prescribed by ANSI Std. 239-18

i

MODIFICATION AND VERIFICATION OF DESIGN SIMULATION FOR THERMOACOUSTIC RESEACH SOFTWARE

Scott B. Curtis
Lieutenant, United States Navy
B.S., Kansas State University, 1992

Submitted in partial fulfillment of the
requirements for the degree of

MASTER OF SCIENCE IN ENGINEERING ACOUSTICS

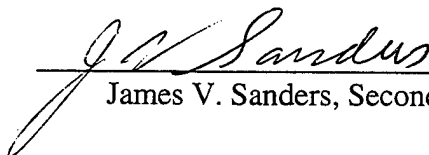from the

NAVAL POSTGRADUATE SCHOOL
March 2000

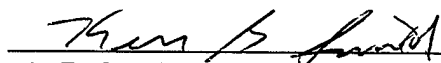Author: _____
Scott B. Curtis

Approved by: _____
Thomas J. Hofler, Thesis Advisor

_____
James V. Sanders, Second Reader

_____
Kevin B. Smith, Engineering Acoustics Chairman

ABSTRACT

This thesis attempts to improve, prepare for release, and verify the accuracy of the expert system code entitled "Design Simulation for Thermoacoustic Research" (DSTAR) created previously by LT Eric Purdy. DSTAR allows a unique new approach for the rapid design and simulation of thermoacoustic devices utilizing a Microsoft Windows™ compliant interface to construct any given thermoacoustic model at runtime. The approach to simulation involves the solution of a one-dimensional acoustic wave equation simultaneously with an energy flow equation from one end of the specified device to the other, including additional lumped elements. The resulting solution is available as both a graphical and text-based output. In order to prepare for release, significant additions to the engine code and interface were completed. Additionally, theoretical results obtained by the DSTAR system code were compared to actual measured values in order to demonstrate potential engineering design applicability.

TABLE OF CONTENTS

I.   INTRODUCTION

Thermoacoustic engines can be classified as either heat pumps or as prime movers. A thermoacoustic heat pump uses a finite-amplitude standing acoustic wave to transport thermal energy incrementally along a thermoacoustic "stack" from one heat exchanger to another. The acoustically generated heat transfer produces a significant thermal gradient over the length of the heat exchanger. This conversion of acoustic energy into stored thermal energy can be used for a wide variety of diverse applications, including refrigeration.

A thermoacoustic prime mover converts stored thermal energy from an external source into kinetic energy in the form of acoustic waves. This process, the reverse of a heat pump, occurs when heat delivered by a heat exchanger causes a temperature differential of sufficient magnitude over the length of a stack, in turn causing an acoustic instability to occur in the internal gas. This instability has an initial exponential rise in amplitude with a growth rate that increases with the temperature gradient and a frequency given by the natural resonance. For example, the resonance may be determined by a quarter wavelength tube resonance. After the initial exponential growth, the amplitude will reach a limit determined by the complex nonlinear interplay between heat-exchanger conduction, acoustic dissipation and loading characteristics.

The primary attraction of thermoacoustic heat engines is that they can be constructed over a range of sizes, allowing for a large variety of applications, and have few or no moving components. When compared to conventional heat engines, they are extremely simple and inherently reliable, and also have the desirable benefit of having no

1

requirement for chlorofluorocarbons (CFC's) or other environmentally damaging substances.

A.   HISTORY

The study of thermoacoustics dates back to the late 1700's, when the experiments of Byron Higgins included the study of oscillations in a large pipe that were excited by a hydrogen flame within the tube. Higgins' work laid the groundwork for the study of pulse combustion which was fundamental to the development of the V-1 "Buzz Bomb" by the Germans in World War II and more peaceful applications such as the Lennox pulse combustion furnace in 1982.

Thermoacoustics became a quantitative field in the late 1800's when glassblowers discovered that a hot glass bulb attached to a cooler glass tube would emit a sound. Sondhauss studied this phenomenon and determined a relationship between the frequency of the sound and the dimensions of the tube. A qualitatively correct explanation of the Sondhauss effect was given by Lord Rayleigh in his text "Theory of Sound" (1896). A significant leap forward occurred in 1962 when Carter discovered that the placement of a heat exchanger (referred to as the stack) within a Sondhauss tube would significantly improve its thermodynamic performance. In 1968 Nikolaus Rott presented a theory applicable to the study of both thermoacoustic heat pumps and prime movers in the low-amplitude (linear) regime. The Rott equations are still the primary mathematical descriptions used in the study of thermoacoustics [Ref. 1].

B. THERMOACOUSTIC ENGINE MODELS AND DSTAR

Rott's theoretical work, combined with modern computers, has allowed the development of an extensive library of computer codes to model acoustic heat engines. Typically, these codes are developed for the analysis of a specific thermoacoustic device; with any configuration or operating change the code itself must be changed to reflect the new situation. This development of new code for every change is time consuming and can be technically difficult.

In 1998 at the Naval Postgraduate School, Purdy and Hofler created a new expert system code to model thermoacoustic devices. This code, titled Design Simulation for Thermoacoustic Research (DSTAR) is a Windows™-compliant graphical based program that provides a flexible and powerful tool for the design and analysis of thermoacoustic heat engines. The code allows the analysis of the thermoacoustic-wave and energy-transfer equations from the beginning to the end of a thermoacoustic heat engine, on a component-by-component basis. This approach allows the user to change the configuration and parameters of the individual components of the heat engine "on the fly" with DSTAR recalculating the effect of the changes on the overall solution of the heat engine. DSTAR was a significant step forward in the field of thermoacoustics. It is a powerful and easy to use tool for the design of future thermoacoustic heat engines.

C. OBJECTIVE

The goal of this thesis was to modify and verify the DSTAR code and make it releasable to the professional. The modifications include improvements to the user

interface, the addition of outputs directly importable to commercial CAD programs, corrections to the early DSTAR object model, support software including extensive online help files, an installer, and the creation of a website from which the code can be downloaded. Experimental verification of the DSTAR solutions for existing thermoacoustic heat engines was performed, thereby giving a comparison of the performance of an existing thermoacoustic device to the measured values.

D.   SCOPE

Chapter II, a qualitative and quantitative description of the foundations of basic thermoacoustic theory, will give the reader insight into the rationale and procedures used in the solutions of the thermoacoustic equations. This will also lend understanding of the limitations of the DSTAR code.

Chapter III details the construction and operation of the DSTAR program as developed by Purdy and Hofler. It serves to give the reader a basic overview of the interface, abilities, and limitations of the program. A basic description of the object model used is provided, giving an understanding of future expandability of DSTAR. This section will also address the improvements to the initial code and additions in preparation for release.

Chapters IV and V provide the reader with an overview of the parameters to be measured, and the techniques used, in order to verify the thermoacoustic solutions generated by DSTAR. A description of the equipment used is provided, including

measurement limitations, experimental techniques, and discussion of the parameters selected for measurement.

Chapter VI provides the verification of the theoretical results generated by DSTAR through comparison of measured experimental values. After reading this section, the reader should have an impression of the power and limitations of the DSTAR program. A comparison of the values for thermoacoustic onset and cessation temperature, operating frequency, radiated power, and efficiency generated by DSTAR to those measured will be made using a Mini-Hofler Tube. This device combines physical simplicity with thermoacoustic complexity sufficient to stress the computational ability of DSTAR.

Chapter VII offers conclusions regarding the potential applicability of the DSTAR code and its effect on the future development of thermoacoustic engines. Recommendations for future improvements to DSTAR are made.

II. THERMOACOUSTIC HEAT ENGINES

A complete analytical analysis of the thermoacoustic process is provided by Swift [Ref. 1, 3] and is used as the basis for the description provided in this thesis.

A.   EFFICIENCY AND THE CARNOT CYCLE

All reversible heat engines operate in one of two modes -- as a prime mover or a heat pump. As a prime mover, the application of thermal energy from two reservoirs of differing temperature will generate useful work within the engine. As a heat pump, the application of work to the engine will cause heat energy to flow from a region of lower temperature to one of higher temperature.

The First and Second Laws of Thermodynamics place a limit on the efficiency of any process involving the use of heat engines. This limit depends solely on the temperatures of the two reservoirs used by the heat engine; the high temperature reservoir with a temperature of T_h, and the cold reservoir with a temperature of T_c. The associated heat energy flows into and out of the heat engine are given as the heat flow to or from the hot reservoir, Q_h, and to or from the cold reservoir, Q_c. The resulting work of, or by, the heat engine is expressed by the symbol W.

The First Law of Thermodynamics states that for any process, the total energy of the system must be conserved, i.e.

$$Q_h - Q_c = W \tag{2-1}$$

The Second Law of Thermodynamics states that the total entropy generated by any real process must be positive or zero. Understanding that entropy can be expressed as

7

proportional to the heat flow to a reservoir divided by the temperature of that reservoir, the 2nd Law can be expressed as

$$\frac{Q_c}{T_c} - \frac{Q_h}{T_h} \geq 0 \quad \text{(Prime Mover)} \tag{2-2}$$

or

$$\frac{Q_h}{T_h} - \frac{Q_c}{T_c} \geq 0 \quad \text{(Heat Pump)} \tag{2-3}$$

For the case of a prime mover, the efficiency is

$$\eta = \frac{W}{Q_h} \tag{2-4}$$

which, when combined with equations (2-1) and (2-4) reduces to

$$\eta \leq \frac{T_h - T_c}{T_h} \tag{2-5}$$

The Carnot efficiency represents the upper bound for any prime mover can achieve.

In the case of an engine operating as a heat pump, the power performance is referred to as the Coefficient of Performance (COP) and is given by:

$$COP = \frac{Q_c}{W} \tag{2-6}$$

which, when combined with equations (2-1) and (2-6), reduces to

$$COP_c \leq \frac{T_c}{T_h - T_c} \tag{2-7}$$

The Carnot Coefficient of Performance represents the upper bound for the COP for any heat pump.
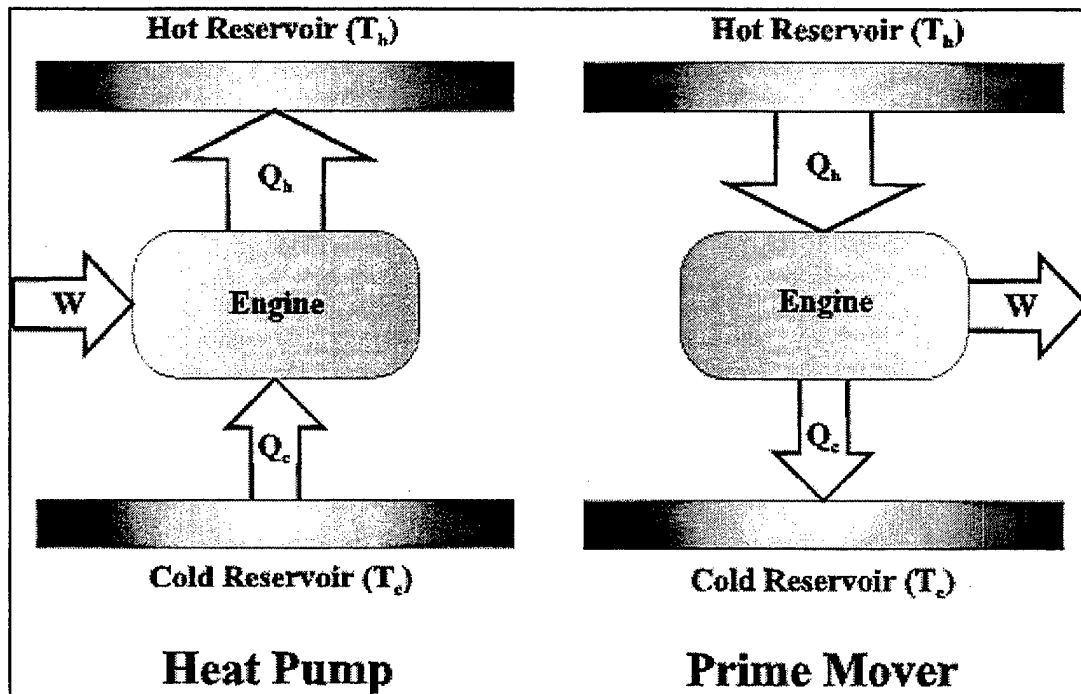
Figure 2-1: Heat Engine Operation

The Carnot Cycle, as shown in Figure 2-2, represents the ideal thermodynamic cycle in which the net increase in entropy over the cycle in zero. For this ideal cycle, there are two isothermal steps in which work and heat flow into or out of the engine, and two adiabatic steps in which compression and expansion of the fluid medium occurs. When carried out at near equilibrium conditions, the total increase in the entropy of the system during the expansion step is exactly equal to the total drop in the entropy during the compression step. Any real thermodynamic engine generating useful work will never operate under these conditions, and will therefore have a net increase in the total entropy over one cycle. It is for this reason that the Carnot Cycle represents the upper bound of the possible efficiency of any heat engine, be it a prime mover or a heat pump.

9
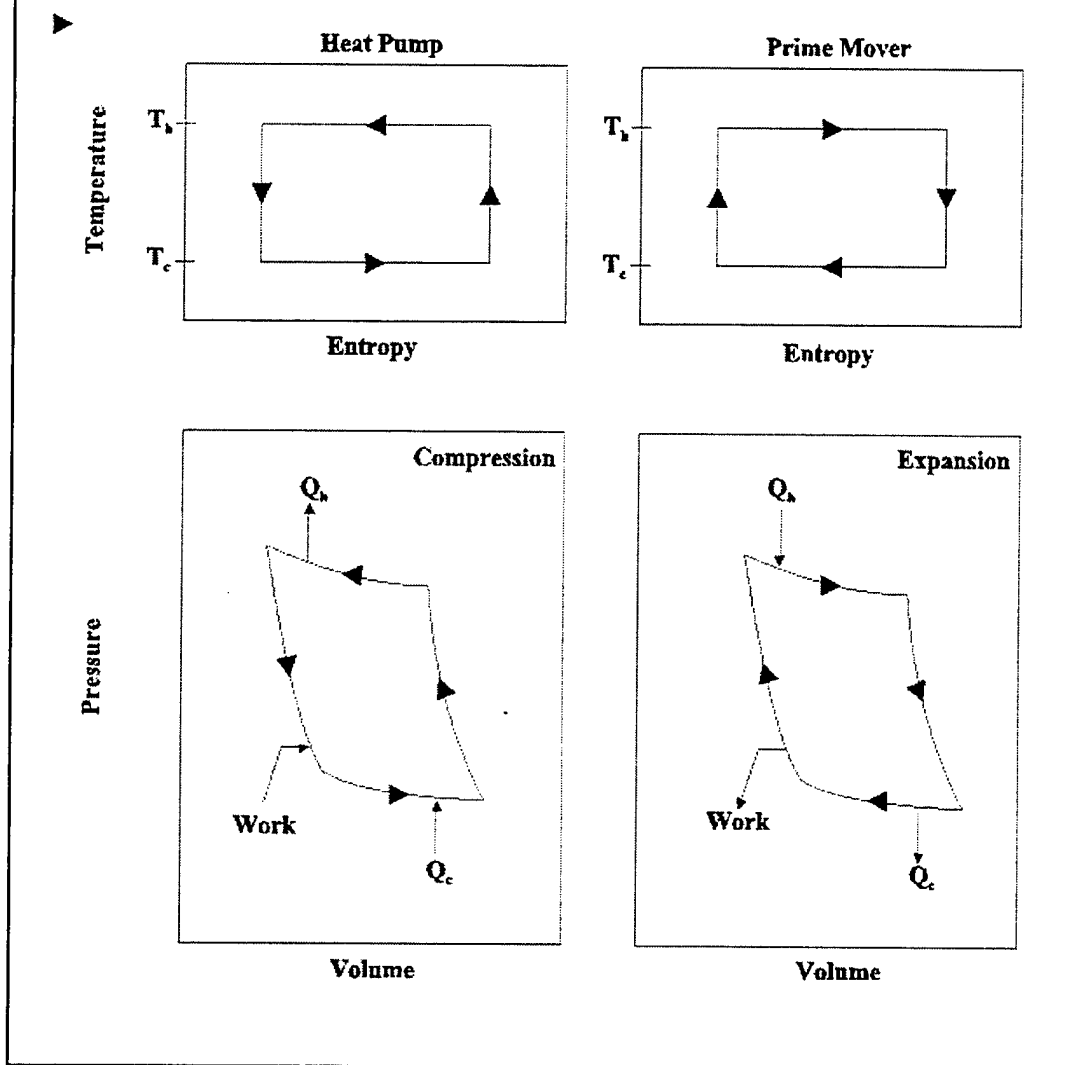
Figure 2-2: The Carnot Cycle temperature-entropy (T-S) and pressure-volume (P-V) diagrams for both the prime mover and heat pump. The near equilibrium state of the cycle ensures that the total change in entropy over one cycle is zero. This yields the rectangular plot in the T-S diagram, and ensures that the total work added to or removed from the engine is equal to the area enclosed by the P-V cycle.

B.   THERMOACOUSTIC ENGINES

1.   Engine Design

A thermoacoustic engine converts thermal energy from a high temperature heat source into useful work, in the form of acoustic power, while exhausting waste thermal

10

energy to a cold heat sink. To accomplish this task, several components are required. The first is a means for the high thermal energy to enter the engine. This is referred to as the hot heat exchanger. Second, a means of expelling waste thermal energy from the engine to the cooler heat sink is required. This is called the cold heat exchanger. Between the two heat exchangers is a set of precisely spaced metal plates referred to as the stack. The purpose of the stack is to provide a means of temporary heat storage and to provide a smooth temperature gradient from the hot heat exchanger to the cold heat exchanger. The final basic component, and the most important factor in determining the operation of the engine, is the resonator tube. This tube determines the frequency of the acoustic energy produced by the engine. In an open tube configuration, as shown in Figure 2-3, the lowest resonant mode is a quarter wavelength with pressure anti-nodes at the closed end and pressure nodes at the open end. This configuration ensures that the fundamental will have a wavelength approximately four times the length of the tube. Other configurations are possible, including a closed end resonator with pressure nodes at both ends producing acoustic power at a wavelength two times the physical length of the tube.

2.   Thermoacoustic Requirements and the Thermodynamic Cycle

To qualitatively understand the operation of a thermoacoustic heat engine, the Lagrangian point of view should be adopted. By following a finite parcel of the gas the thermoacoustic effect is easily demonstrated. A more rigorous, Eulerian approach is provided by Swift [Ref. 1].
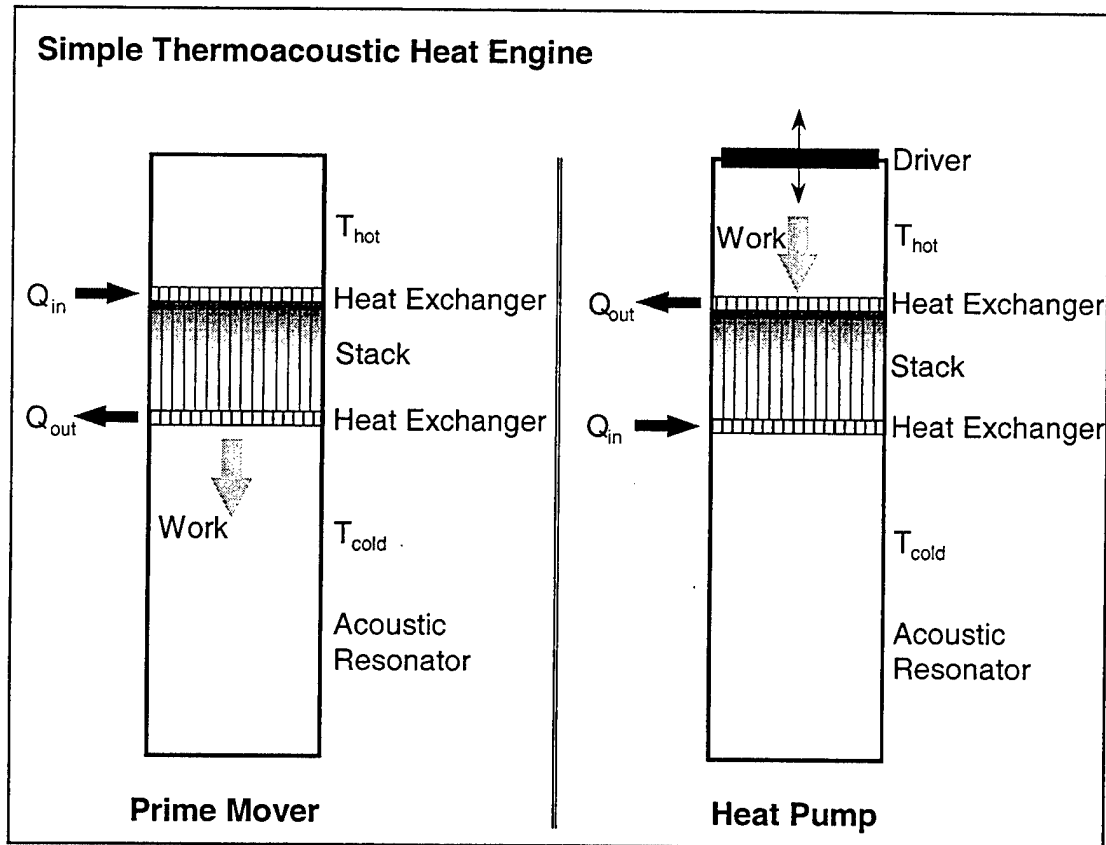
Figure 2-3 Simple Thermoacoustic Engine (from Purdy [Ref. 2], pp. 9)

Although the acoustic oscillations within the resonator are sinusoidal, the cycle is best explained by approximating the sinusoid with a square wave. The cycle then consists of two reversible adiabatic steps and two irreversible constant pressure steps, identical to the conventional Brayton cycle [Ref. 4].

In a conventional heat engine, piston movement and valve actuation are mechanically controlled by coordinated crankshafts and camshafts. In a thermoacoustic heat engine, there are no mechanical elements to ensure the proper phasing of the cycle. The key to phasing within a thermoacoustic heat engine is the presence of two thermodynamic media, the fluid and the stack plate. The change in the temperature of the

gas parcel as it moves along the plate comes from the adiabatic compression and expansion of the parcel and from the presence of the plate that is operating at a different temperature than the gas parcel. The heat flow between the gas parcel and the plate does not produce an instantaneous change in temperature, but there is a time delay between the temperature and pressure. To ensure that this time delay is correct, a specific thermal conductivity is required. If the thermal conductivity is too high, the change in temperature of the gas parcel will occur too rapidly, and therefore no time delay will be created. If the thermal conductivity is too small, no appreciable temperature change will occur and the cycle will not be driven. The proper thermal conductivity is related to the thermal penetration depth, δ_κ. The thermal penetration depth is the distance heat diffuses through the fluid medium during a time $1/\omega$, and is defined by

$$\delta_\kappa = \sqrt{\frac{2\kappa}{\omega}}$$
(2-8)

where κ is the fluid's thermal diffusivity [Ref. 5].

A detailed analysis has shown that the optimal spacing of the plates within a stack is approximately $4\delta_\kappa$. This spacing allows the optimal heat transfer from both plates to the fluid trapped between them. An additional consideration is that the plate spacing allows for the required expansion and compression of the fluid so that it can absorb or do work. It was shown by Swift that this is also optimized at one viscous penetration depth [Ref. 5].

ACOUSTIC HEAT ENGINE CYCLE (HOFLER TUBE - PRIME MOVER)
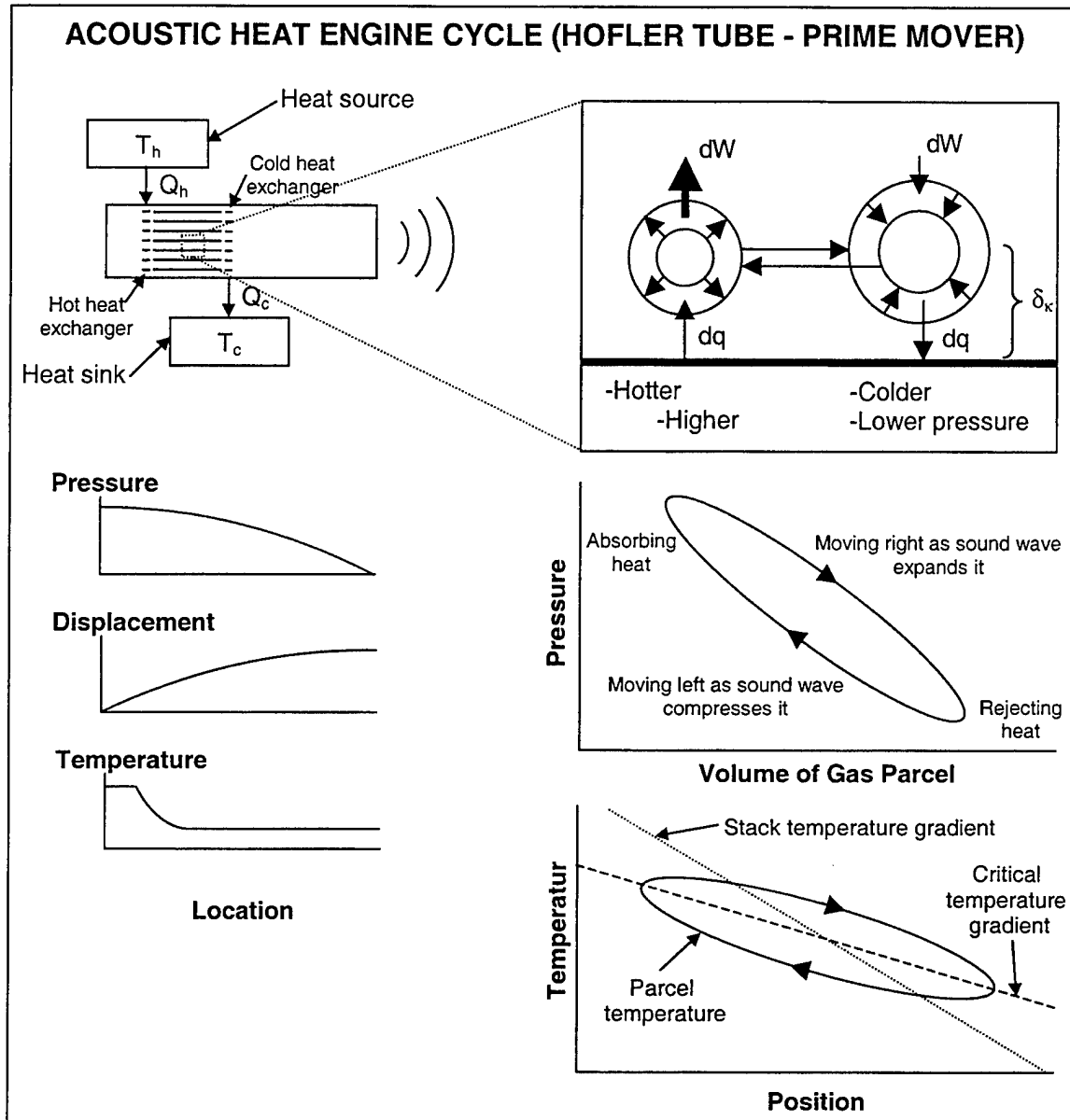
Figure 2-4 The Thermoacoustic Cycle: Shown is the cycle undergone by one infinitesimal parcel of gas. (a) The parcel adiabatically expands and moves to the right, away from the increasing acoustic pressure. (b) The parcel rejects heat energy to the cooler stack plating. (c) The oscillating acoustic pressure compresses the parcel and drives it back to the left. (d) The parcel absorbs heat energy from the hot stack plate. (From Swift [Ref. 1], pp. 23).

Figure 2-4 shows the movement, heat transfer, and volume changes of a parcel of

gas as it moves during one cycle. Initially, the gas parcel is stationed at one thermal

penetration depth from the plate in a region of high acoustic pressure gradient. The high

14

pressure gradient drives the parcel to the right, while at the same time the parcel is absorbing heat from the plate. The combination of the decreasing acoustic pressure and the increase in temperature of the parcel causes its volume to increase during the movement to the right. As the parcel moves toward the cooler portion of the stack plating, it begins to release heat energy into the plate. The oscillating acoustic pressure creates a region of reverse high pressure gradient at this point, driving the parcel back to the left toward the region of high temperature while at the same time compressing the parcel. Once the parcel returns to the initial point at which the cycle began, it is in its initial state and begins the cycle again. Each iteration of the cycle causes a small amount of heat energy is transferred from the region of high temperature to the region of low temperature. In the next section, it will be shown how this effect can be exploited to create useful thermoacoustic engines, whether operating as a prime mover or as a heat pump.

3.   Heat and Work Flow in the Short Engine

The simplest model of a thermoacoustic engine that can still be applied to actual design is the short engine. The model of the short engine makes a number of assumptions. The first of these is the "short stack approximation" that assumes that the length of the stack is much less than the wavelength of the resonator's fundamental mode. The second approximation is that the temperature gradient between the hot and cold heat exchangers is much less than the absolute operating temperature. The model

includes viscosity, longitudinal thermal conductivity, finite heat capacity of the plate, and multiple plates within the stack.

There are two mechanisms by which the oscillating gas parcel undergoes a temperature change. The first is the adiabatic compression and expansion of the parcel, as described by the ideal gas law. The second is due to the flow of heat energy between the parcel and the plate. The first mechanism will occur independent of the temperature gradient of the fluid and the plate. The second can only occur due to a temperature difference between the fluid and the plate. When the temperature change of the parcel due to compression and expansion equals the temperature change of the plate over the range that the parcel has moved, no net heat transfer occurs between the gas parcel and the stack plate. This critical temperature gradient, ∇T_{crit}, is of great importance since it marks the transition of the engine from prime mover to heat pump. If the temperature of the fluid after adiabatic compression is greater than that of the adjacent plate, there will be a net transfer of heat energy out of the fluid. Therefore, the parcel experiences thermal contraction at high pressure. This state means that work is being done on the parcel, signifying a prime mover operation. Conversely, if the temperature of the fluid after adiabatic compression is less than that of the adjacent plate, there will be a net transfer of heat energy into the fluid. This causes thermal expansion at high pressure where the fluid is doing work on the system (i.e. driving thermal energy from cold to hot), thereby acting as a heat pump.

Up until this point, the operation of the engine has been analyzed from the interaction of a single gas parcel with the stack plate. During operation, the actual

displacement of the gas volume is extremely small. Therefore, a single gas parcel will cause a net heat transfer over an infinitesimally small distance. As Figure 2-5 shows, the only temperature differential of interest in the operation of the engine is between the hot and cold heat exchangers, which are attached to the ends of the stack. Within the stack, the point that one gas parcel deposits heat is also where the adjacent parcel absorbs its heat energy. This continuum of gas parcels causes a continuous heat flow along the stack with the net differential being the sum of all of the individual parcel contributions. Only at the ends of the stack, where there is no longer an adjacent plate area for the parcel to absorb or release heat energy, can useful heat flow occur.
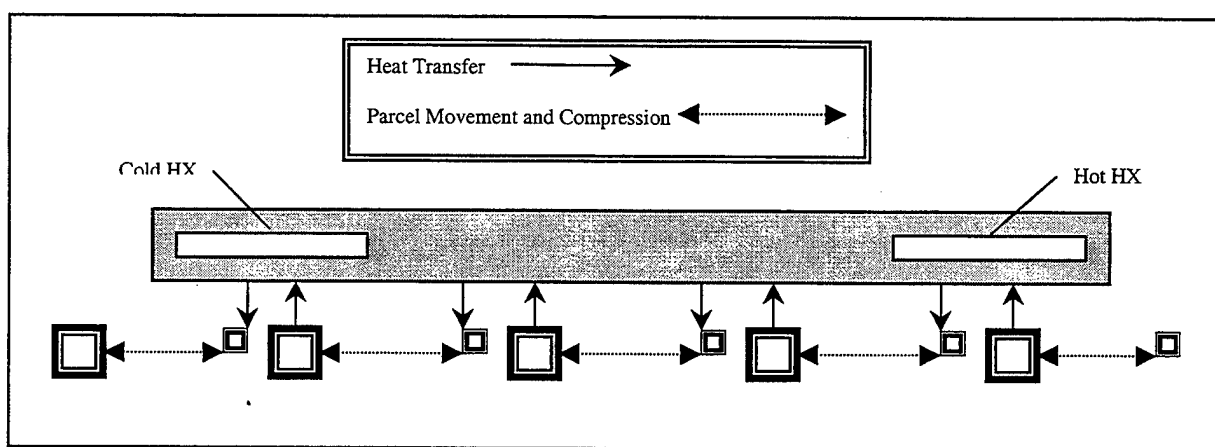
Figure 2-5 Multiple oscillating fluid parcels operating along a stack plate with heat exchangers at either end. Each parcel acts to move thermal energy from the hot heat exchanger to the cold heat exchanger (prime mover operation shown), in a "bucket brigade" action.

4.   The Rott Wave and Energy Flow Equations

To go beyond the basic qualitative description of the theory of thermoacoustic heat engines, quantitative description through the use of the Rott equations is required. The derivation of these equations is lengthy and was provided by Swift [Ref. 5] and will

17

not be developed here. These equations, as modified by Swift, form the foundation of numerical models of thermoacoustic devices of which DSTAR is one.

The first equation is the equation developed by Rott and Swift for acoustic propagation within a channel formed by parallel plates where the plates may have a temperature gradient. This equation serves to describe the acoustic wave within the stack, which is closely approximated by such a channel [Ref. 3,5], and is given by

$$\left(1+\frac{(\gamma-1)f_\kappa}{1+\varepsilon_s}\right)p_1 + \frac{\rho_m a^2}{\omega^2}\frac{d}{dx}\left(\frac{1-f_v}{\rho_m}\frac{dp_1}{dx}\right) - \beta\frac{a^2}{\omega^2}\frac{f_\kappa-f_v}{(1-\sigma)(1+\varepsilon_s)}\frac{dT_m}{dx}\frac{dp_1}{dx} = 0 \qquad (2\text{-}9)$$

where

$$
\begin{aligned}
f_v &= \frac{\tanh[(1+i)y_0/\delta_v]}{(1+i)y_0/\delta_v} \\
f_\kappa &= \frac{\tanh[(1+i)y_0/\delta_\kappa]}{(1+i)y_0/\delta_\kappa} \\
\varepsilon_s &= \frac{\sqrt{K\rho_m c_p}\ \tanh[(1+i)y_o/\delta_\kappa]}{\sqrt{K_s\rho_s c_s}\ \tanh[(1+i)y_o/\delta_s]} \\
\sigma &= c_p\mu/K = v/\kappa \\
\delta_\kappa &= \sqrt{2\kappa/\omega} \\
\delta_v &= \sqrt{2v/\omega}
\end{aligned}
\qquad (2\text{-}10)
$$

The above equation is a general form that is applicable for both liquids and gases as the propagation medium. However, if the medium is assumed to be an ideal gas, the ideal gas law may be applied. This, combined with the definition of a set of non-dimensional state variables, reduces Equation (2-7) to [Ref. 3,5]

$$\left[1+\frac{(\lambda-1)f_\kappa}{1+\varepsilon_s}\right]\mathbf{P} + \left[(1+f_v)+\frac{1}{2}(1+\beta_r)(f_v+\tanh^2\eta_0-1)-\frac{f_\kappa-f_v}{(1-\sigma)(1+\varepsilon_s)}\right]\frac{d\mathbf{T}}{d\mathbf{X}}\frac{d\mathbf{P}}{d\mathbf{X}} + (1-f_v)\mathbf{T}\frac{d^2\mathbf{P}}{d\mathbf{X}^2} = 0 \qquad (2\text{-}11)$$

where

$$\eta_0 = (1+j)(y_0/\delta_\nu).$$

(2-12)

The capitalized bold-face variables are normalized or non-dimensional variables, and are defined in Appendix A. Equation (2-11) allows the complex state variables of pressure and pressure gradient or velocity to be determined if the temperature gradient is known.

The second parameter of interest for the development of thermoacoustic models is the 2nd order enthalpy, H_2. This energy flow equation, as developed in Ref [5] is

$$\dot{H}_2 = \frac{\Pi y_0}{2\omega\rho_m} \text{Im}\left[\frac{d\tilde{p}_1}{dx} p_1 \left(1 - \tilde{f}_\nu - \frac{T_m\beta(f_\kappa - \tilde{f}_\nu)}{(1+\varepsilon_s)(1+\sigma)}\right)\right]$$
$$+ \frac{\Pi y_0 c_p}{2\omega^3\rho_m(1-\sigma)} \frac{dT_m}{dx} \frac{dp_1}{dx} \frac{d\tilde{p}_1}{dx}$$
$$\times \text{Im}\left[\tilde{f}_\nu + \frac{(f_\kappa - \tilde{f}_\nu)(1+\varepsilon_s f_\nu/f_\kappa)}{(1+\varepsilon_s)(1+\sigma)}\right]$$
$$- \Pi(y_0 K + lK_s)\frac{dT_m}{dx}$$

(2-13)

The final local state variable of temperature can be determined by DSTAR with Equation 2-14. If the energy equation is rearranged to express the temperature derivative with respect to position in terms of the constant energy term and acoustic variables, and ideal gas law and non-dimensional variables are used, the result is

$$\frac{d\mathbf{T}}{d\mathbf{X}} = \frac{\mathbf{T}\text{Im}\left[\frac{d\tilde{\mathbf{P}}}{d\mathbf{X}}\mathbf{P}\left(1 - \tilde{f}_\nu - \frac{f_\kappa - \tilde{f}_\nu}{(1+\varepsilon_s)(1+\sigma)}\right) - \mathbf{H}_2\right]}{\frac{\mathbf{T}}{(\lambda-1)(1-\sigma)}\left|\frac{d\mathbf{P}}{d\mathbf{X}}\right|^2 \text{Im}\left[1 - \tilde{f}_\nu - \frac{(f_\kappa - \tilde{f}_\nu)(1+\varepsilon_s f_\nu/f_\kappa)}{(1+\varepsilon_s)(1+\sigma)}\right] + \mathbf{K}}$$

(2-14)

19

With the development of the wave and energy equations, as described above, mathematical techniques must be used to determine the solutions applicable to the device of interest. To properly solve the equations as initial value problems or boundary value problems, numerical techniques must be used since closed form solutions are not available.

III. PROGRAM ORGANIZATION AND OPERATION

DSTAR provides a dynamic simulation of a thermoacoustic heat engine. It allows the user to modify and change the parameters of the individual thermoacoustic components "on the fly" without recompiling any portion of the computational code when the simulation is executed. This section provides the reader with an overview of the operation and organization of the interface and features of DSTAR as developed by LT Eric Purdy, and modifications made as part of this thesis.

A. THE DSTAR OBJECT MODEL

DSTAR is programmed in the C++ language with the use of Microsoft Visual C++. The object oriented nature of the C++ language, coupled with the graphical interface support of the Microsoft Visual C++ development environment, provides an inherently organized, stable, and expandable program. The primary components of any object oriented code are the main classes that define the operations performed by the code. There are numerous classes used in DSTAR, but there are several primary ones that are the key to performing the dynamic simulation. Further information on the class structure of DSTAR is provided in the Purdy thesis [Ref. 2].

The highest level object modeled is encapsulated in the class CTAEngine, which represents the thermoacoustic engine itself. This object defines functions and variables that are present in any thermoacoustic device, and are required to compute a solution to the wave and energy equations. During the solution of a boundary value problem,

CTAEngine serves to iterate the solution until the boundary conditions are satisfied [Ref. 2].

The key to solving the wave and energy equations of an entire arbitrary thermoacoustic device is to break it into individual components and solve the equations for each. An example of this is shown in Figure 3-1 where a simple thermoacoustic tube is broken into its constituent parts, and in Figure 3-2 where the general CTAModule representation is given. Through the use of the CTAEngine class, these individual components are joined to provide a solution. The CTAModule class serves as the next level of abstraction under the CTAEngine class and represents each component of the thermoacoustic engine through the definition of an object derived from CTAModule. It is within this class that the solutions are generated using either the numerical Runge-Kutta Cash-Karp method, or established analytical solutions when they exist [Ref. 2].

The CTAElement class provides the individual variables that define the physical structure of any thermoacoustic component. For example, a heat exchanger will have variables of radius, length, plate spacing, thermal conductivity, etc. Each of these parameters are defined as objects of the CTAElement class. Additional values that are not exposed to the user are defined within this class, including strings that define the components and boolean flag values. It is these objects defined by the CTAElement class that provide the output values to the user [Ref. 2].

The CTAEngine, CTAModule, and CTAElement classes discussed provide the primary mechanism for the simulation of any user-defined thermoacoustic device. DSTAR consists of many more classes in addition to these, including classes that control

the graphical user interface (GUI), provide the numerical methods for the solution of the

differential equations and enable the execution of multiple functional accessories to the
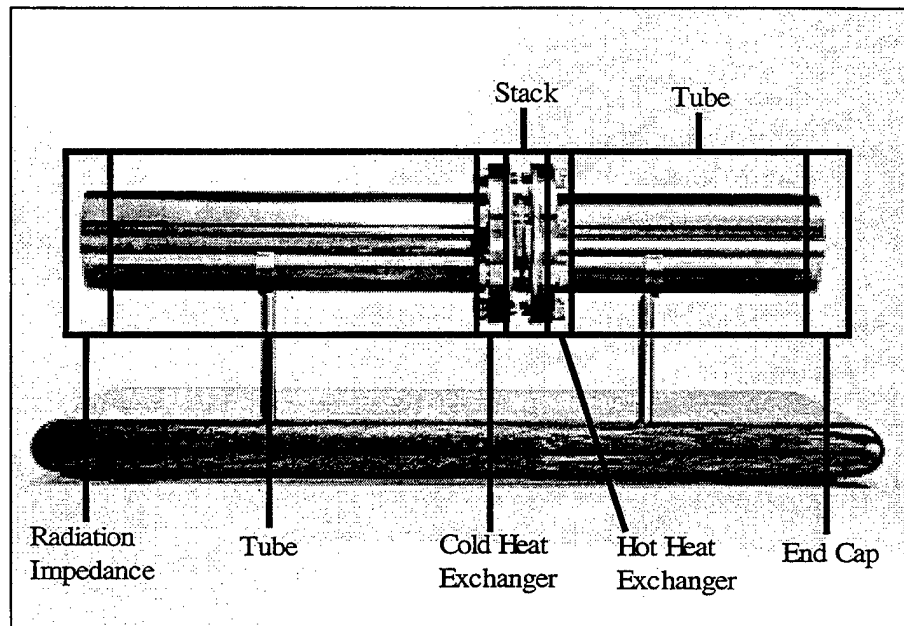
program.

Figure 3-1: Simple Thermoacoustic Engine and Individual Components (From Purdy [Ref. 2], pp. 29)
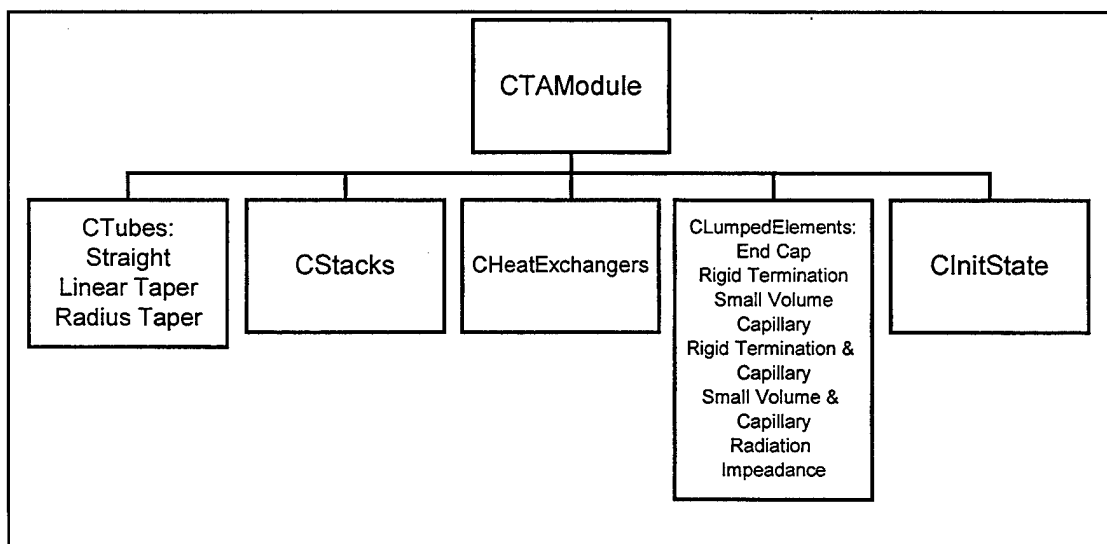

Figure 3-2: CTAModule Class and Derived Components (From Purdy [Ref. 2], pp. 29)

B.   THE GRAPHICAL USER INTERFACE

The DSTAR Graphical User Interface (GUI) provides the framework through which the user can modify the parameters that define the thermoacoustic device, and also provide means of displaying the resulting data in a clear and concise format. The DSTAR GUI is organized using Windows™ standards, and therefore minimizes any steep learning curve that would be encountered by novice users of the program.

1.   Main Program Window

The DSTAR main window is shown in Figure 3-3. The main window has been maintained essentially in the original condition as developed by Purdy, with the exception of the addition of the **Options** pulldown menu to the standard menu bar at the top of the window. Immediately below the menu bar is the DSTAR toolbar that provides shortcuts for commonly used functions, as well as the means to execute the computation of either initial value problem (IVP) or boundary value problem (BVP) solutions. The majority of the window is taken up with five tabbed portions that provide the primary means by which the user can create and modify a thermoacoustic device. Finally, at the bottom of the window, a status bar provides information regarding program status, as well as basic description of menu and toolbar functions.

a.   Menu Commands

The **File** menu, shown in Figure 4-4, contains all of the standard Windows functions related to storage and retrieval functions, as well as the **Exit** function and a list of recently used files. When the **Save** function is selected, all current variable values and

model geometry are saved to disk, and can be accessed at any later time through the

Open function. In addition to these standard functions, the **File** menu also contains

functions that allow the user to **Export Solution Data to File**, as well as to generate a

Computer Aided Drafting (CAD) compatible graphical output file through the **Export**
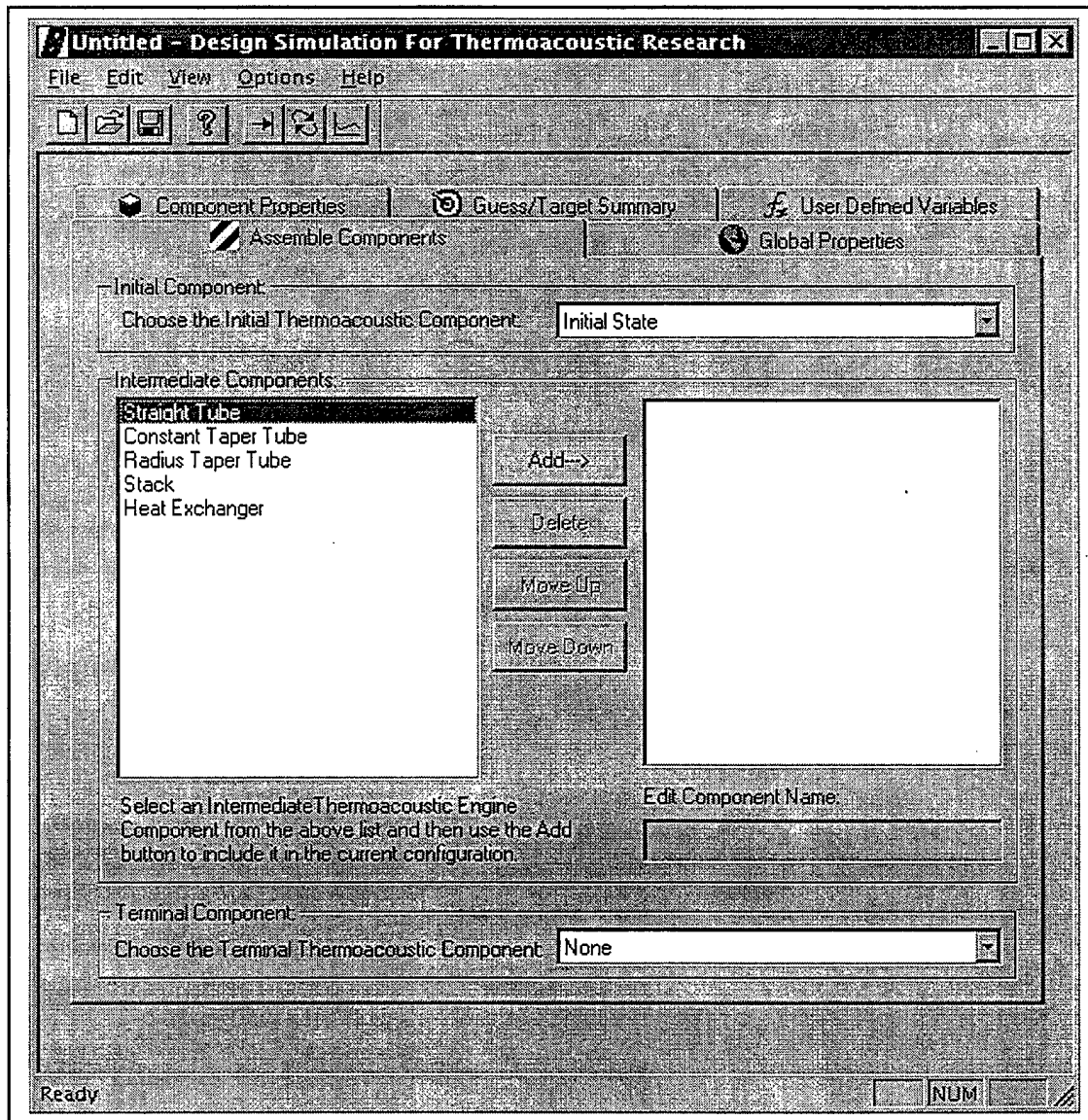

Figure 3-3 Main Program Window

CAD Data to File function. The **Options** menu described in the Purdy thesis [Ref. 2]

has been moved from the top-level **File** menu, to a separate top-level menu of its own.

The **V̲iew** menu allows the user to select whether the Toolbar and Status Bar are

available for viewing. Additionally, the menu enables the user to view the Output

Window at any time.
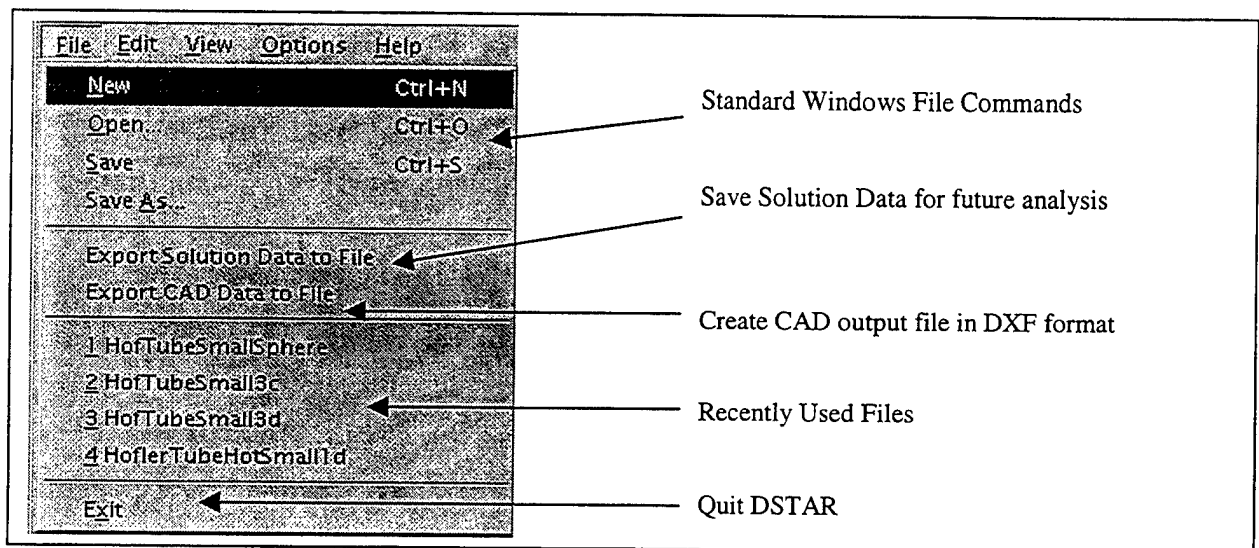
Figure 3-4 Modified **F̲ile** Menu

The **O̲ptions** menu contains user selections that control the computational

parameters that DSTAR uses to obtain a solution to the engine model. The options

available for user manipulation at this time include the parameters used during the

numerical solution of the initial and boundary value problems, and are accessed through

the **I̲VP/BVP** selection. These parameters are shown in Figure 3-5, and include

tolerances for the integration solution, step size, and maximum number of steps. DSTAR

default values can be recovered at any time by pressing the **Defaults** button.
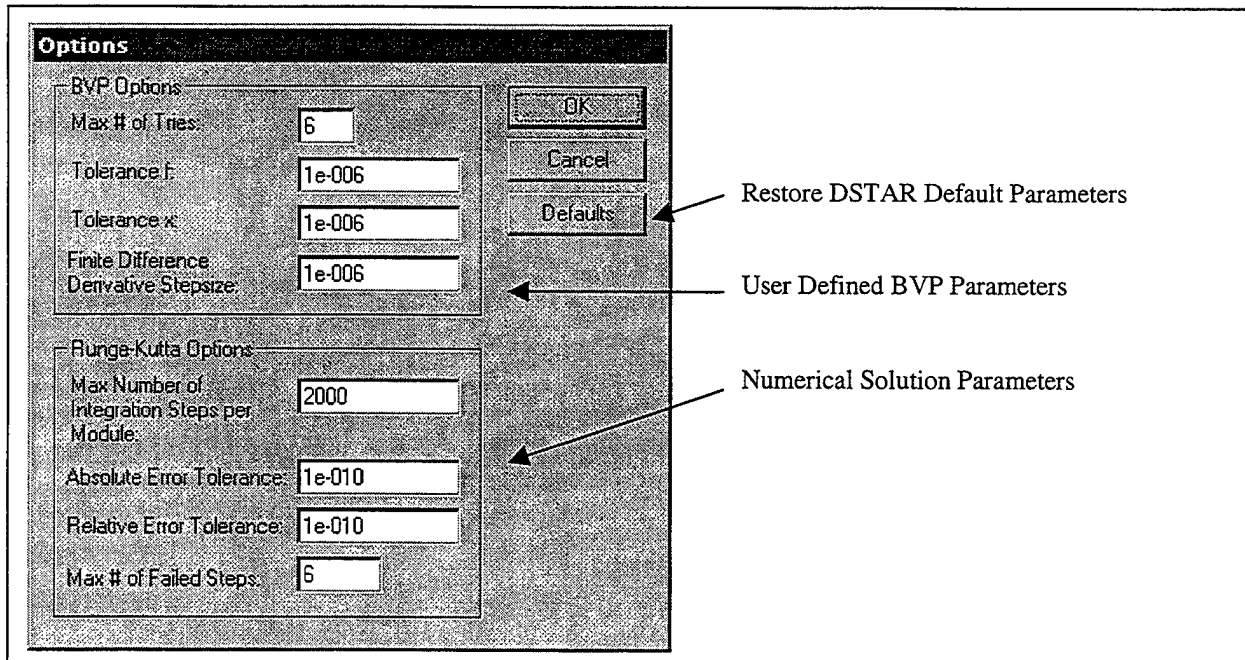
Figure 3-5 Modified **Options** menu

b.   *The Toolbar*

The DSTAR toolbar contains shortcut icons for functions contained within the menu structure addressed in the previous section, as well as the buttons that initiate the calculations of Initial Value Problems (IVPs) or Boundary Value Problems (BVPs). The toolbar is normally located at the top of the DSTAR main-program window immediately below the menu functions, but it can be hidden or displayed using commands contained within the **View** menu. The toolbar maintains the original appearance, as developed by Purdy, however the functionality of the **Help** button has now been instituted. The toolbar is shown in Figure 3-6.

27

Figure 3-6. The DSTAR Toolbar and Icon Functions (From Purdy [Ref. 2], pp. 43).

c. Tabbed Multi-Function Views

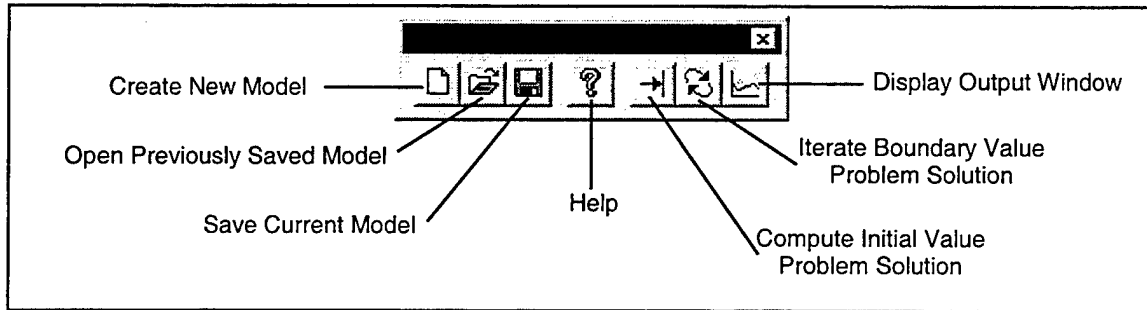The multi-function tabbed views of DSTAR constitute the primary means by which the user creates the thermoacoustic device, defines component and environmental parameters, and sets unknown boundary condition guesses and targets. There are five tabs, each providing different features. Detailed characteristics and operation of the individual tabbed view can be found in the Purdy thesis [Ref. 2]. The information provided here is given as an overview of the DSTAR interface, and a review of changes made to the original tabbed views detailed in the Purdy thesis [Ref. 2].

The **Assemble Components** tab allows for the component-by-component design of the users thermoacoustic device. The tab, shown in Figure 3-7 contains a pulldown list of initial and terminal components that the user can select from. Possible components include commonly designed components, such as end caps, rigid boundaries, user defined lumped elements with or without capillaries, and a spherical volume. Additionally, the user may define the **Initial State** that defines a set of known local state variables. Once the initial and terminal components are chosen, the user can select any combination of intermediate components, provided that simple thermoacoustic design is followed (i.e.

28

two heat exchangers with a stack between them). Once the intermediate components are

chosen, the user must edit the component names to differentiate between different

components with similar structure (i.e. Hot and Cold heat exchangers).
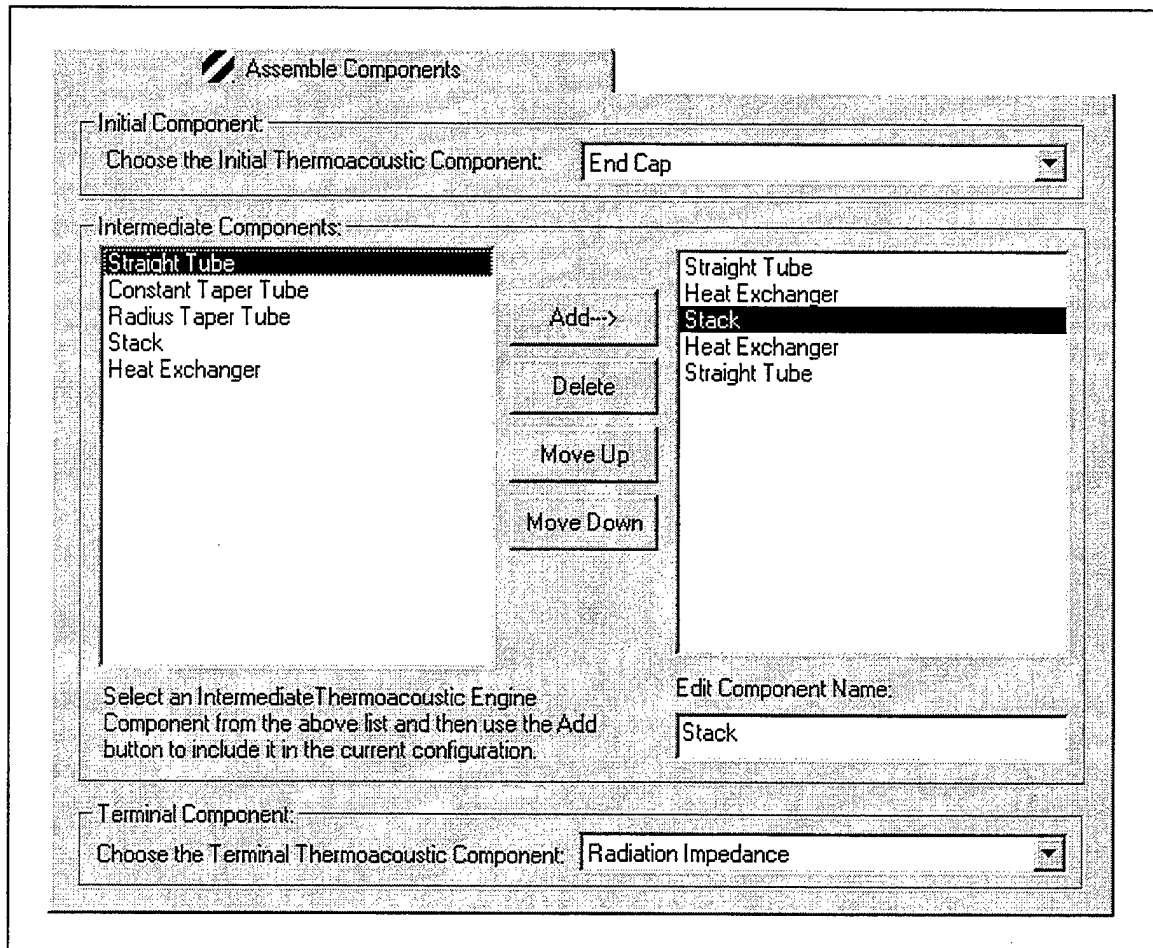
Figure 3-7. The Assemble Components tab.

The **Global Properties** tab, as shown in Figure 3-8, provides the user interface

through which environmental and operating properties can be input and edited. The

columns on the right side of the interface allow the user to designate a given variable as a

guess, a target, or an optimized quantity. The optimized quantities option is not currently

available, but will be instituted in future versions of DSTAR. Shown is the tab used

during simulation of a small Hofler tube. The frequency parameter is set with an initial

guess of 1000 Hz, and scale values corresponding to the component simulation are given

on the right, with all global values being saved to a file, *globalstemp.gvf*, for future use.
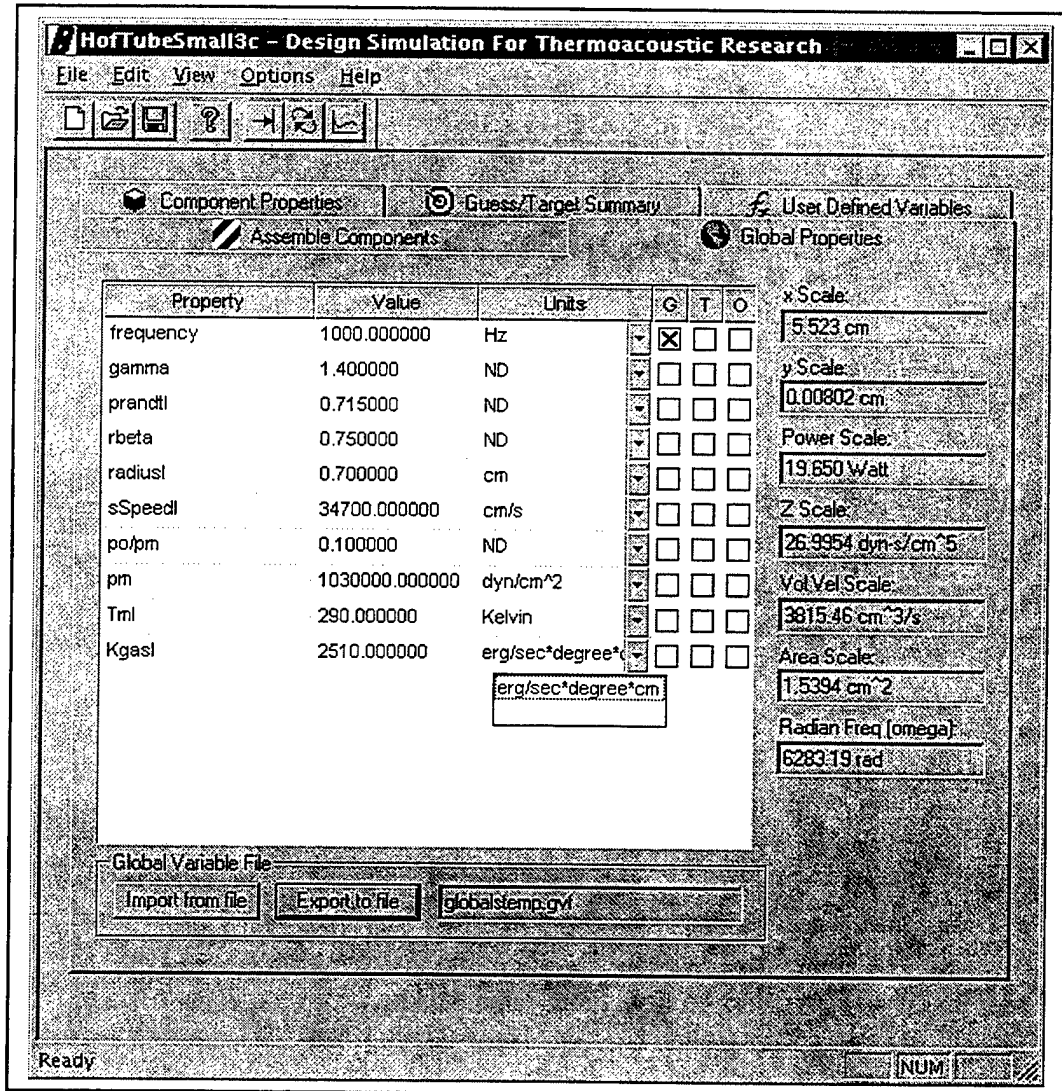
Figure 3-8: Global Properties Tab

The **Component Properties** tabbed view provides the ability to define all

relevant parameters for each of the individual components that make up the complete

thermoacoustic device. This view is shown in Figure 3-9, with the stack component from

the small Hofler tube selected. Each component has it's own list of properties and

values, all of which must be edited by the user prior to commencing the simulation. The

properties can be defined by the user, or entered as guesses or targets. Only those
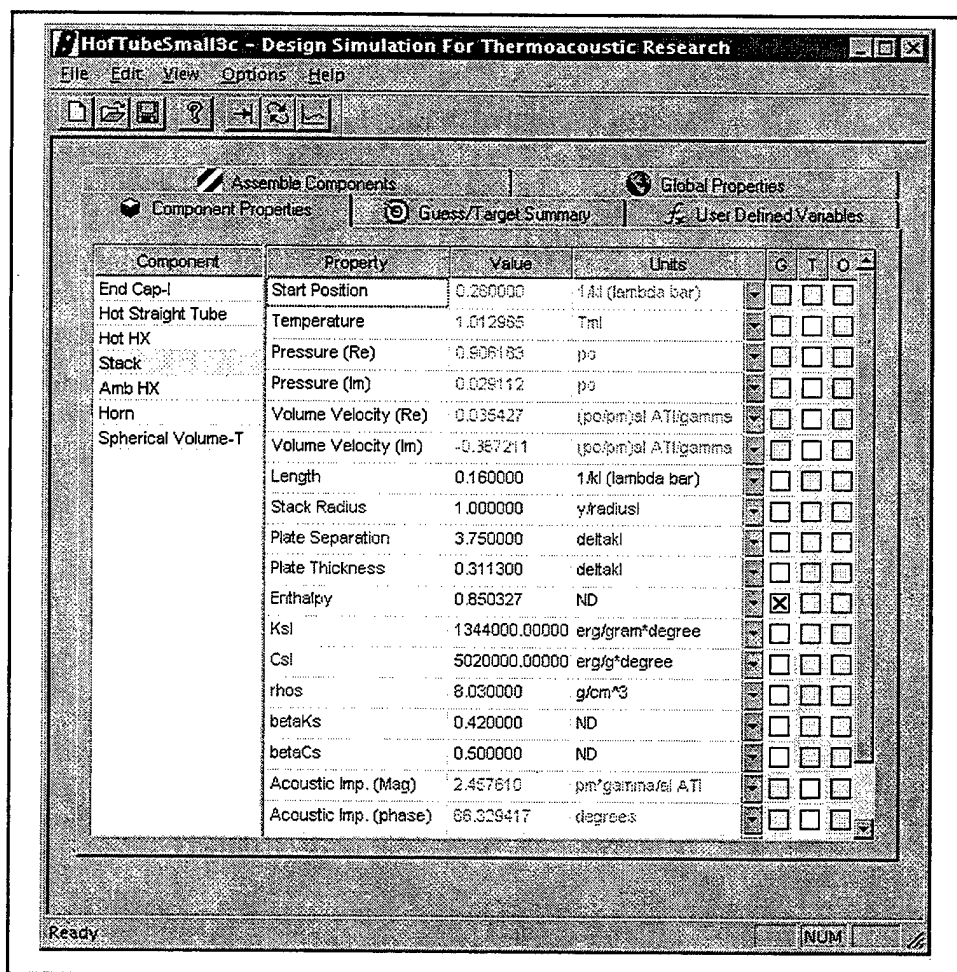
Figure 3-9: Component Properties Tab

properties that are displayed in green may be edited, with grayed values typically being non-user editable and determined by DSTAR.

The **User Defined Variables** tab allows the user to create any variable that can be defined using the local state quantities that DSTAR determines during the solution to the wave and energy flow equations. This allows the user to have DSTAR determine quantities relevant to a specific device, such as COP for a refrigerator or efficiency for a prime mover. Further detail on user-defined variables can be found in the Purdy thesis [Ref. 2].

The final tab is the **Guess/Target Summary** that displays a list of all variables that have been selected as targets and guesses for boundary conditions. For the Runge-Kutta numerical method used by DSTAR to compute a valid solution, the number of guesses and targets must be the same. This tab provides a convenient means of verifying this prior to attempting to determine a solution.

2.   Output Window

After all required information has been input into DSTAR, and a solution is calculated using either the IVP or BVP button, a successful solution will be displayed in the Output Widow. This window provides a graphical and text-based output of all relevant global, component, and user-defined parameters. The graphical portion in the upper left of Figure 3-10, allows the user to quickly determine if the solution is valid and as expected. In addition to acoustic parameters, a plot of the radius of the thermoacoustic

device is provided, which serves as an invaluable tool to determining whether the solution is reasonable.

On the right side of the window is a list of the input and derived global properties, and a detailed list of individual component design geometry and operating parameters. These values can be saved to disk using the **Save Output Text** button. A detailed explanation of the individual component properties can be found in References 1-5.
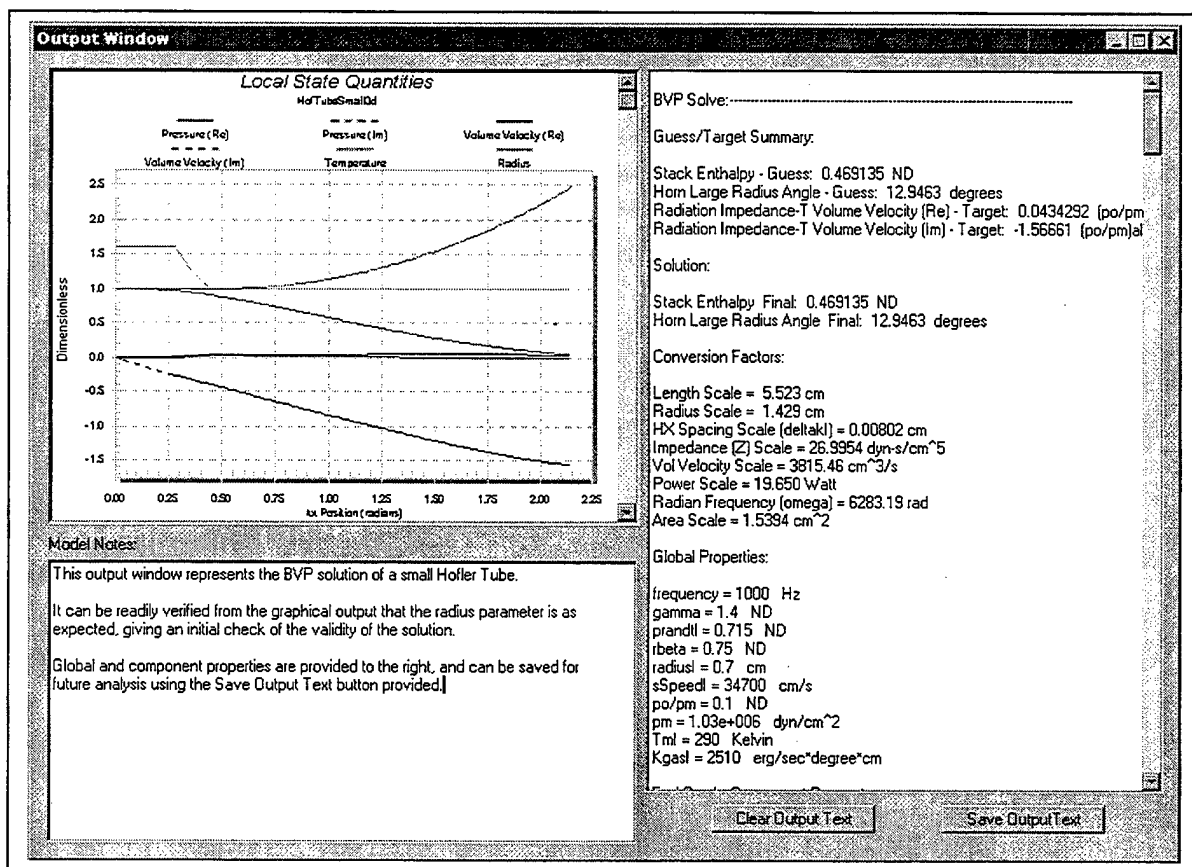
Figure 3-10: Output Window

C.   SOLUTION METHODOLOGY

DSTAR is capable of determining engine design solutions using initial value or boundary value methodology, depending on the state of the known input quantities as

33

entered by the user. When solving an initial value problem, DSTAR solves the system of

steady state first order differential equations corresponding to the one-dimensional wave
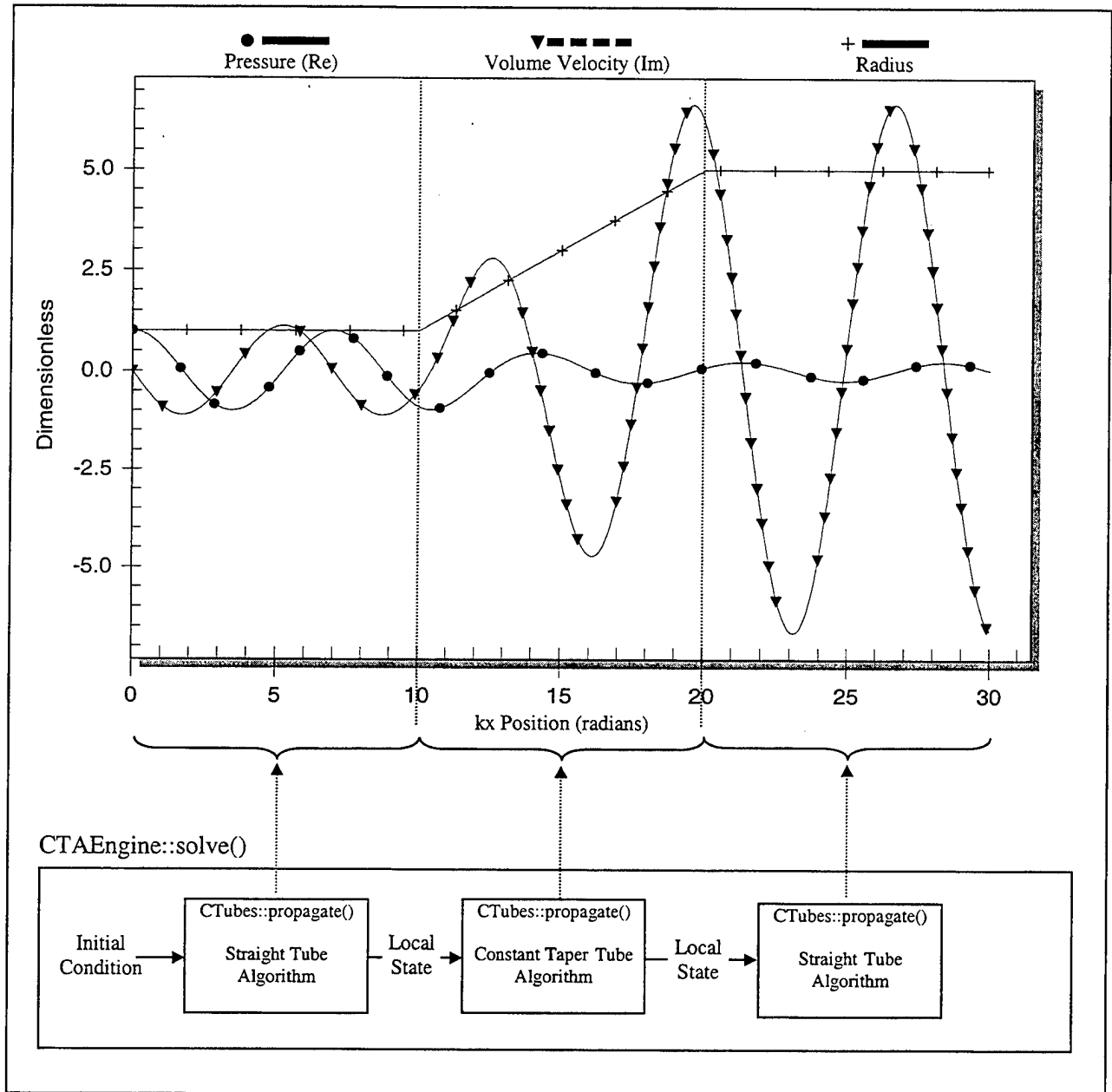
Figure 3-11: DSTAR computation of an Initial Value Problem, showing the output and the CTAEngine method *solve()* (from Purdy [Ref. 2], pp. 35).

34

equation for each component. When the solution to one component is achieved, those values are applied to the initial condition of the next adjacent component, for which another solution is generated. This methodology is applied further throughout the device, until a continuous solution is developed for the entire thermoacoustic engine. This overall solution method is accomplished through the use of the CTAEngine method *solve()* [Ref. 2].

The method *solve()* makes use of the *propagate()* function from each CTAModule object representing an individual thermoacoustic component, such as the stack or heat exchanger. The solution to the system of equations is computed by iterating through an array of CTAModule derived objects, calling the *propagate()* function for each. When a solution to each is determined, the values are passed to the next object in the array as initial conditions, and the method is repeated. In this manner, a solution to the entire CTAModule object is determined, at which point the solution is passed to the next CTAModule object in line (i.e. stack, heat exchanger, tube, etc) as initial conditions, and the process is repeated. When the solution for the final component is obtained, a continuous solution to the wave and energy equations has been determined, and the process is complete. Figure 3-11 displays a block diagram example of the solve() function for a three-tube device and the DSTAR plot that resulted.

Determining the solution to the initial value problem represents only the first step in finding the physical solution to a specific device. In order to determine this solution, boundary values are applies, and the numerical methods previously discussed are applied. The first step in the multivariate Newton-Raphson numerical method used by DSTAR is

```
┌─────────────────────────────────┐
│  CTAEngine::constructVectors()  │
└─────────────────────────────────┘
                │
                ▼
┌─────────────────────────────────┐
│      CTAEngine::mnewt()         │
└─────────────────────────────────┘
                │
                ▼
┌─────────────────────────────────┐
│      CTAEngine::solve()         │
└─────────────────────────────────┘
```

$|\mathbf{F}| \leq tolf$ — yes → solution complete

no

calculate finite difference Jacobian

CTAEngine::luDecomp()
CTAEngine::luSolve()
$\mathbf{J} \cdot \delta\mathbf{x} = -\mathbf{F}$

$|\delta\mathbf{x}| \leq tolx$ — yes → solution complete

no

max number of tries exceeded — yes → solution failed

no

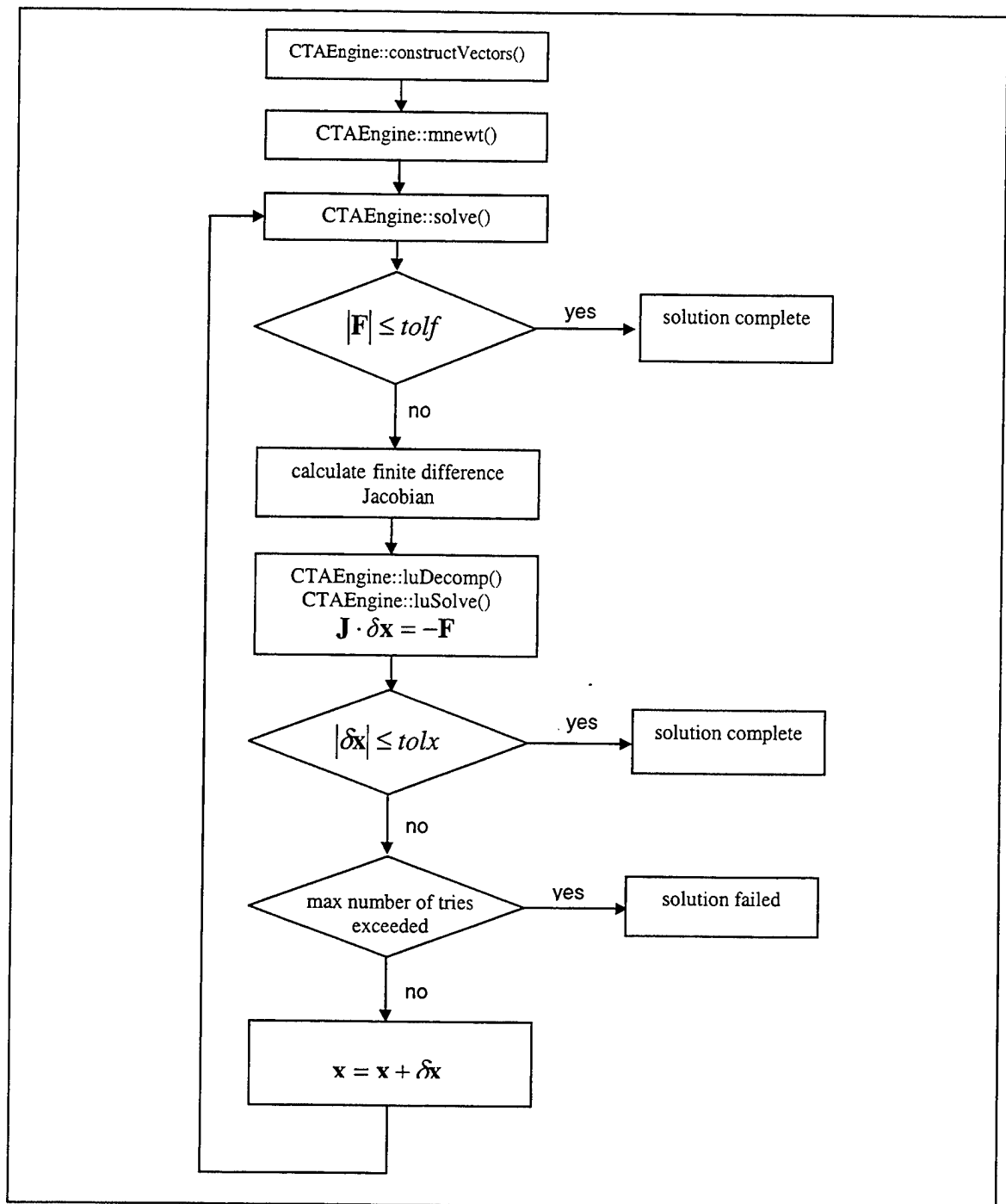$\mathbf{x} = \mathbf{x} + \delta\mathbf{x}$

Figure 3-12: DSTAR Boundary Value Problem Methodology (From Purdy [Ref. 2], pp. 37).

36

the determination of the guessed and target values of variables. This data is stored in a vector **x**, and the difference between the guessed values and the computed values stored in the vector **F**.

After the initial value solution is computed, using the initial user-defined guesses, the Newton-Raphson process calls the *solve()* method to compute the first solution iteration. If the vector **F** is sufficiently small, as defined by the user in **IVP/BVP Options**, then the solution is complete. However, it is highly unlikely that the initial guesses were accurate, therefore the Jacobian matrix is calculated using finite difference partial derivatives, and LU decomposition is performed to determine the guess vector change, δx [Ref. 2]. This change is applied to the initial guess, and the process is repeated until the vector **F** is within the user-specified parameters. A flow chart of this methodology is shown in Figure 3-12.

D.   DSTAR HELP FILES

In developing a useful release version of DSTAR, an online help systems is required to ensure that users understand the background and functionality that DSTAR brings to the development and analysis of thermoacoustic devices. Such a help system was not present in the original DSTAR program developed by Purdy, and has been developed entirely as part of the work contained within this thesis. The resulting help system, shown in Figure 3-13, utilizes the Windows standard class *WinHelp()* in order to integrate the system into the pulldown menu system already in place within the DSTAR graphical user interface.
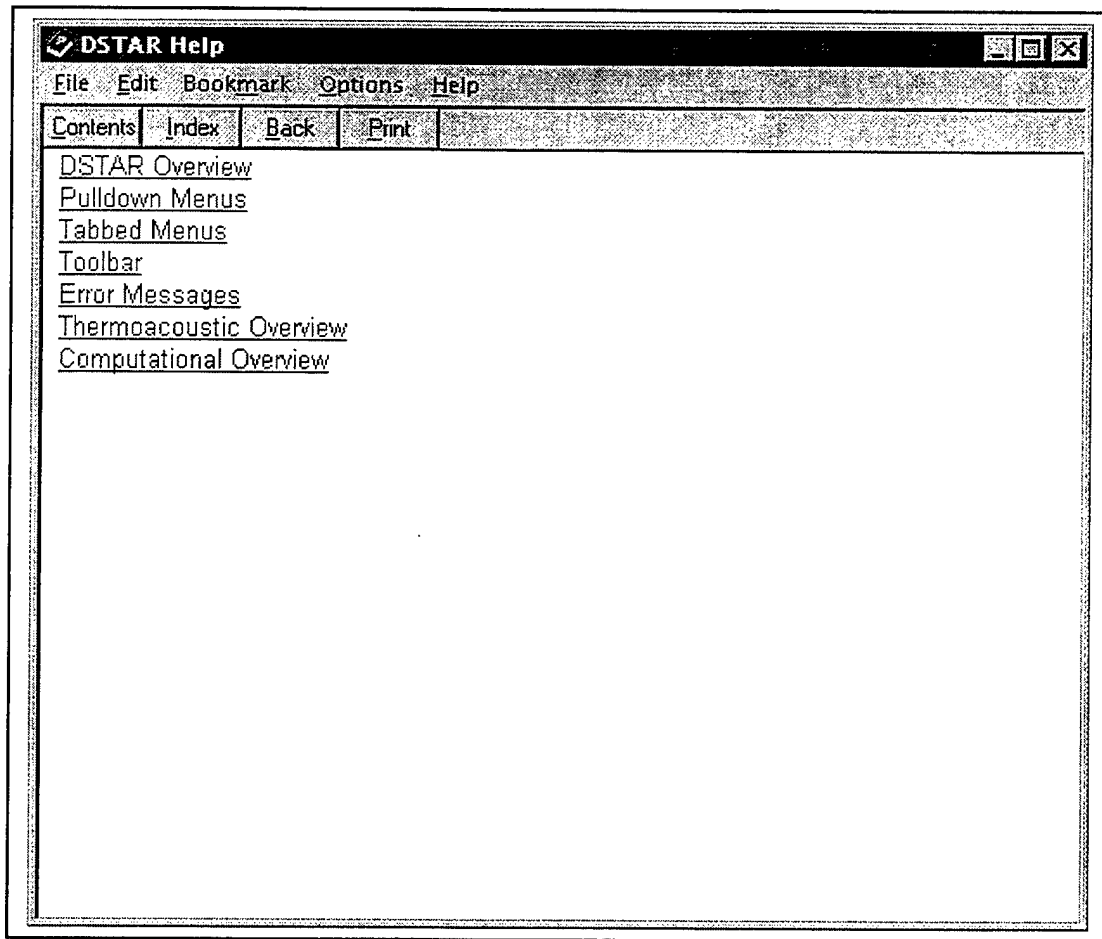
Figure 3-13: DSTAR **Help**

The DSTAR Help system provides an overview of the capabilities of DSTAR

along with a detailed background of the numerical and thermoacoustic principles

employed in solving the wave and energy equations. Additionally, an explanation of the

pulldown menus, tabbed menus, and the toolbar is provided, to give an understanding to

the user in how to employ DSTAR.

In support of future expandability, future additions to DSTAR Help can be easily

made through the use of any editor on the *dstar.hlp* file. This will enable future

enhancements or clarifications to be made and distributed without any changes made to the DSTAR source code.

E.   DXF COMPUTER AIDED DRAFTING OUTPUT

The most significant single enhancement to DSTAR in preparation for release is the inclusion of the ability to generate a computer aided drafting (CAD) quality representation of the device defined by the user and the DSTAR design process. This feature allows the user to utilize DSTAR to create and optimize a thermoacoustic device, and then send the geometry of the design to a DXF formatted file that can be used with most commercial CAD programs. The DXF format is a precision vector graphics format created by AutoDesk Corp. for use in their AutoCAD™ product. It is relatively simple coding scheme based on ASCII sequence of key words, integer codes, and floating point numbers. Without this feature, it would be necessary for the user, or machinist, to draft an engineering print of the design based on the parameters included in the DSTAR Output Window.

In the interest of minimizing processing time and creation of "junk" files, DSTAR will not automatically generate these files unless the user selects the option from the **Export Cad Data to File** option from the **File** menu, as shown in Figure 3-14. When selected, a standard Windows save window will appear, prompting the user for the file name to be saved in *.dxf* format. It is upon the selection of the **Save** button in this window that DSTAR begins generating the CAD output file.
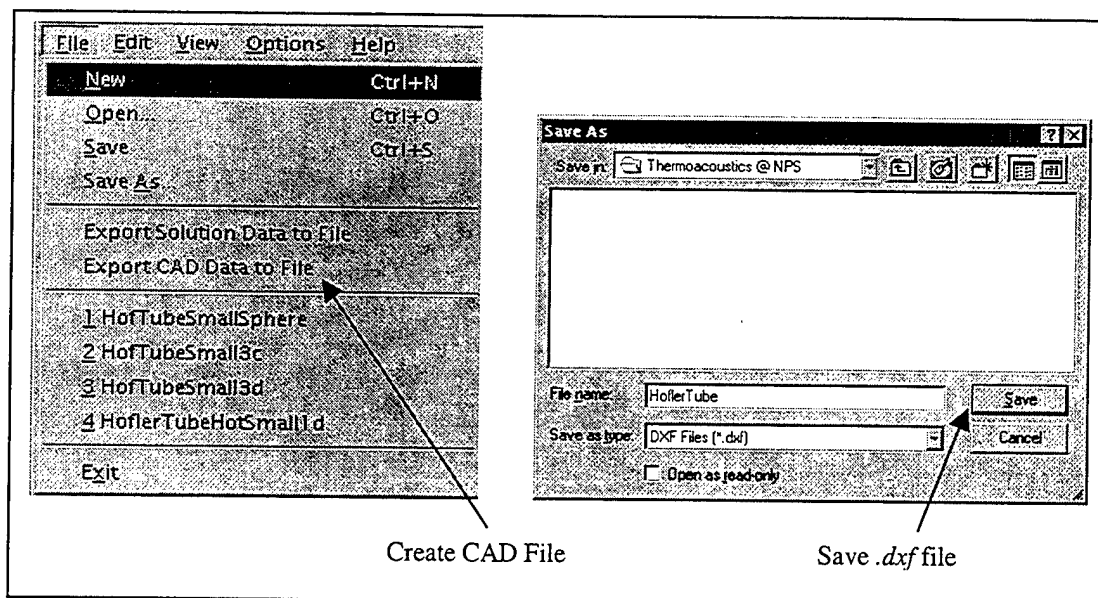
39

Figure 3-14: Creating a *.dxf* Compatible CAD File

In order to create an accurate representation of the geometry of the device created

by the DSTAR engine, the CAD output routine utilizes a component-by-component

methodology similar to that used in the determination of the wave and energy solutions.

To develop the most useful representation of the device, it is required that the numerous

geometric components possible within a single thermoacoustic device be represented in a

"true" fashion. This means arcs and flares are represented by actual arc segments

generated by the CAD program, not just a series of line segments. While to the naked

eye there is no discernible difference between true representation, and that given by very

small line segments, there is a large difference in utility within any commercial CAD

program. The true representation allows the draftsman or machinist to simply select a

component, such as a radius taper or horn flare, and have specific design information

available. This information includes length, width, radius, starting and final angles, and

other information relevant to the construction of the device.

40

To accomplish this, the CAD output routine with DSTAR must be able to identify each component and apply the proper algorithms to construct the *.dxf* representation. The routine accomplishes this by checking first for special components, such as spherical enclosures. If such a component is found, the routine creates the component in the proper format, and then moves to the next. If no unusual component is found, geometric details are checked to determine if the component consists of straight line segments or arcs. The result of this check is further subdivided to determine if the straight line segment is constant or changing radius, and whether the arc segment represents converging or diverging tube geometry. Once the specific geometry of the component is determined, the routine branches to the appropriate construction algorithm where the DXF code is developed. The routine then repeats the process for the next component in line, and includes a check to verify that geometric boundary conditions are met (i.e. the ends of the components meet). After the last component is represented, a centerline axis is drawn, and the file is closed. A flow chart detailing the representation of a device in DXF format is shown in Figure 3-15.

The DXF format file created is compatible with most commercially available CAD programs, such as AutoCAD™, and can also be viewed in most of the numerous shareware CAD viewers available on the Internet. Examples of figures generated by DSTAR are shown in Figures 4-16 and 4-17, viewed using VISUAL CADD™ 3.0 by IMSI. One compatibility exception includes Microsoft Word™, which does support DXF graphics file import, but requires extensive initialization information in the file header that our implementation omits.
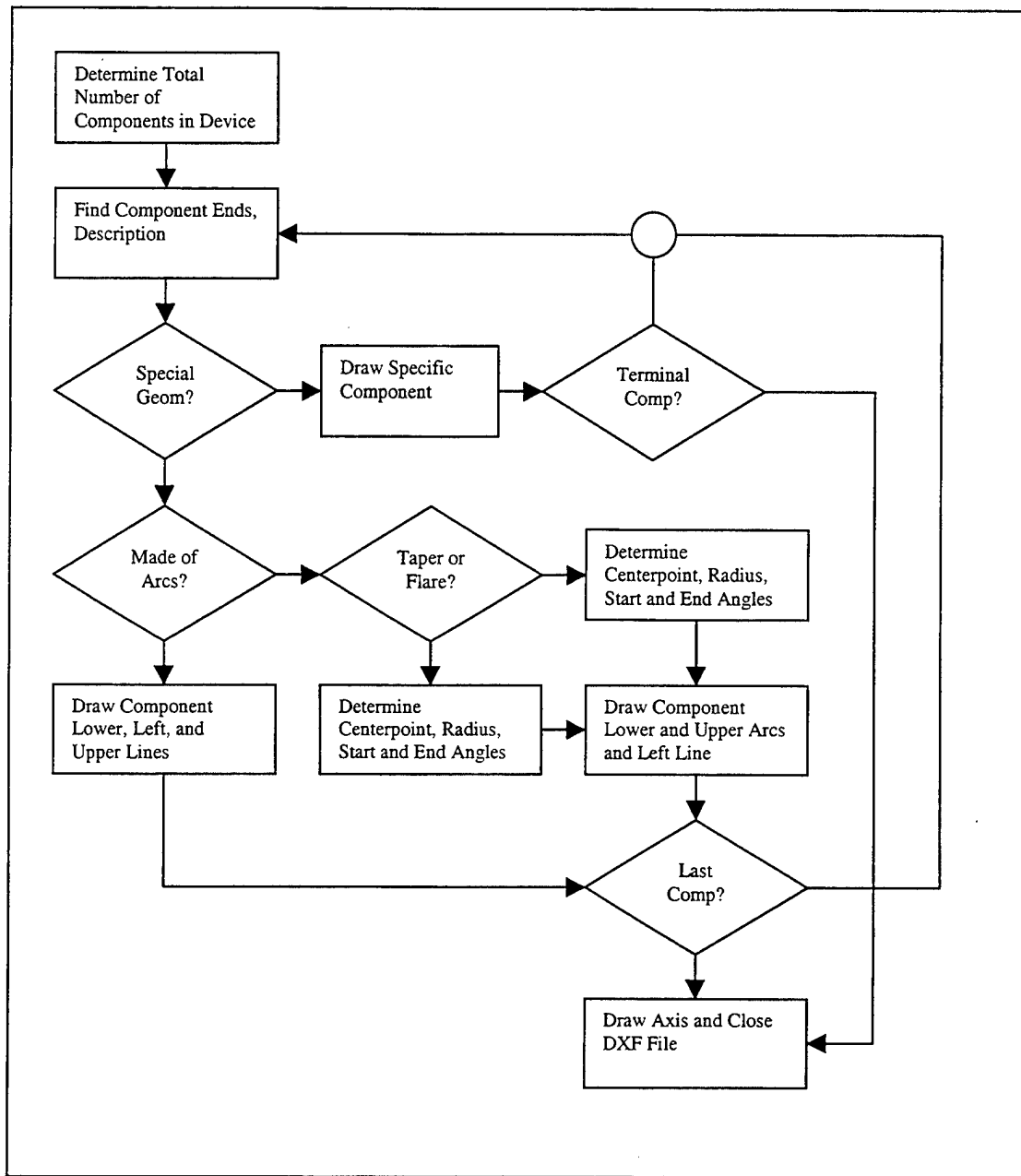
Figure 3-15: CAD Output Routine
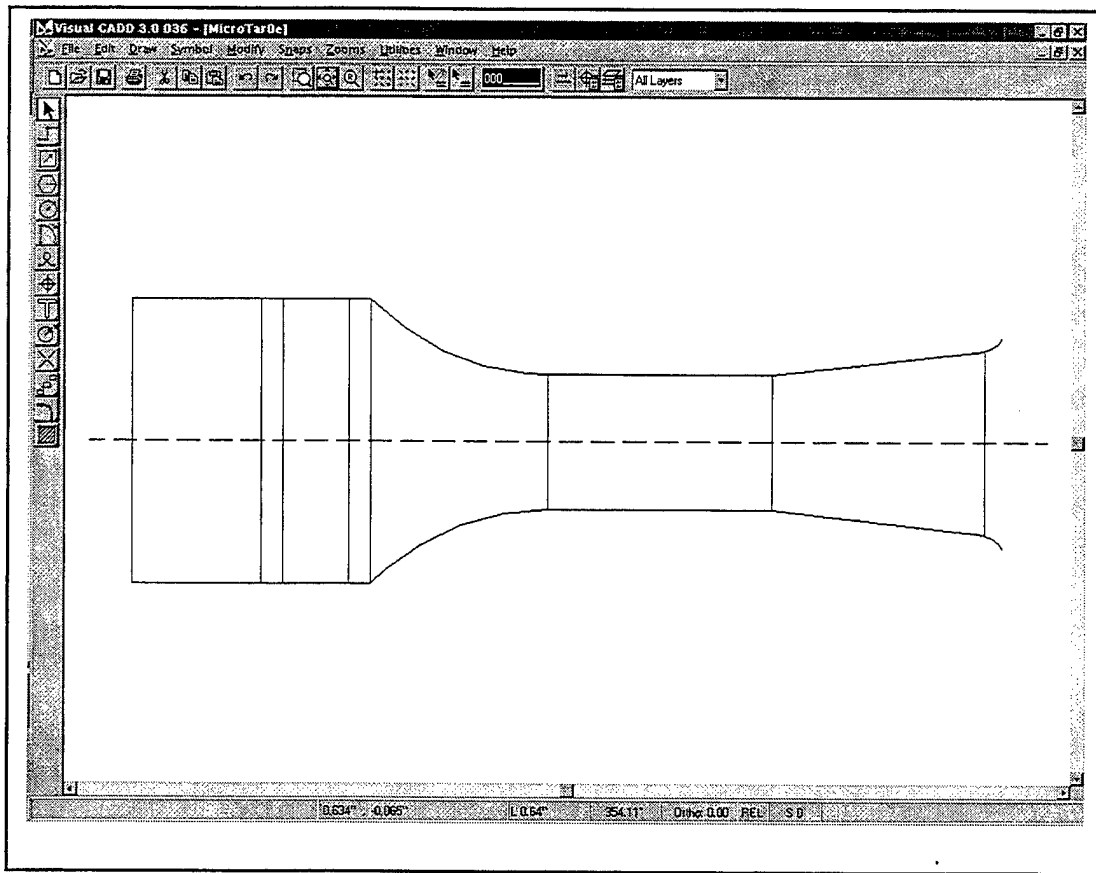
Figure 3-16: DXF CAD Output for Micro-Thermoacoustic Refrigerator
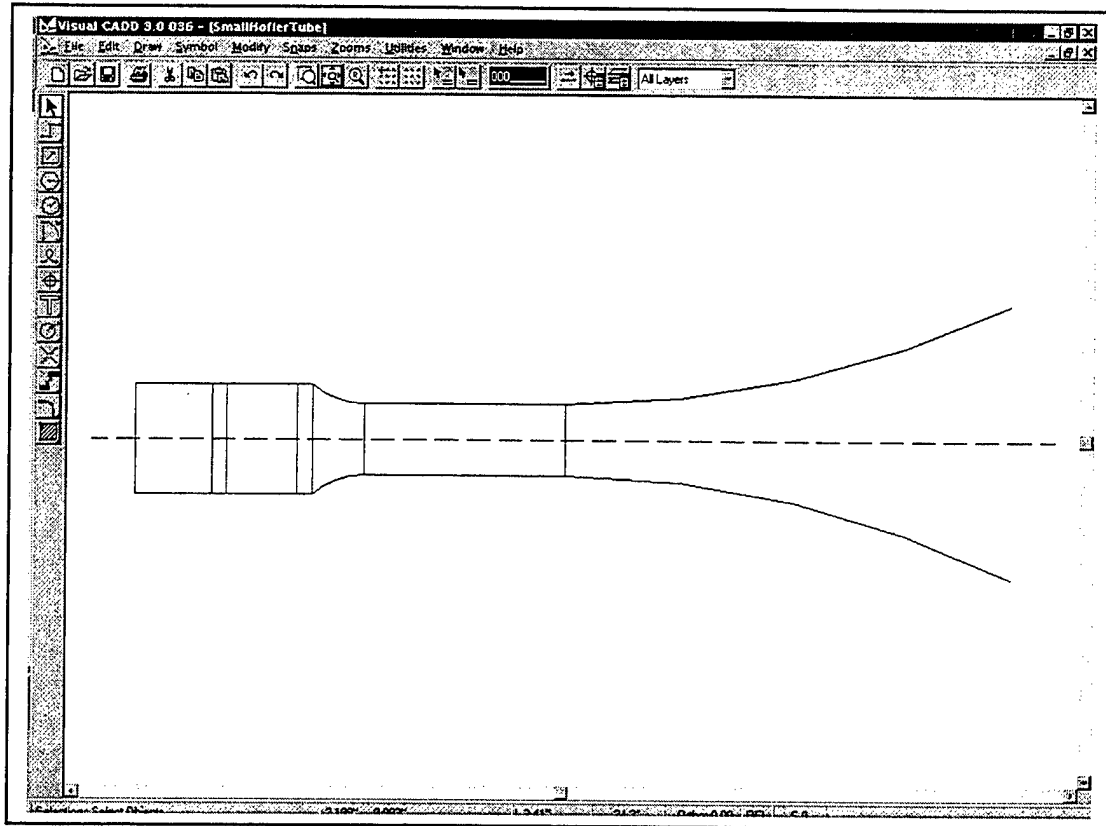
Figure 3-17: DXF CAD Output for Small Hofler Tube

F. INSTALLER

The final release version of DSTAR allows the user to download a single self-extracting ZIP file that contains the installer, DSTAR executable, Help files, sample engine model (.tae) files, and other resources that can be added at any time. The installer, shown in Figure 3-18, allows the user to easily install all DSTAR files to either the default *c:\Program Files\DSTAR* directory, or to any other location. The installer, created using **InstallShield Express™ v5.02**, ensures that all support files are placed in the appropriate DSTAR sub-directory, that required registry entries are made, and that the computer's *Start* menu is updated with shortcuts to the DSTAR executable.

44

Figure 3-18: DSTAR Installer

IV.   MEASUREMENT INSTRUMENTATION

DSTAR provides an excellent tool by which users may create and model thermoacoustic devices. However, in order to serve as a useful tool for creating such devices, the user must have confidence that the device will behave as predicted. To this end, existing simple thermoacoustic devices were modeled by DSTAR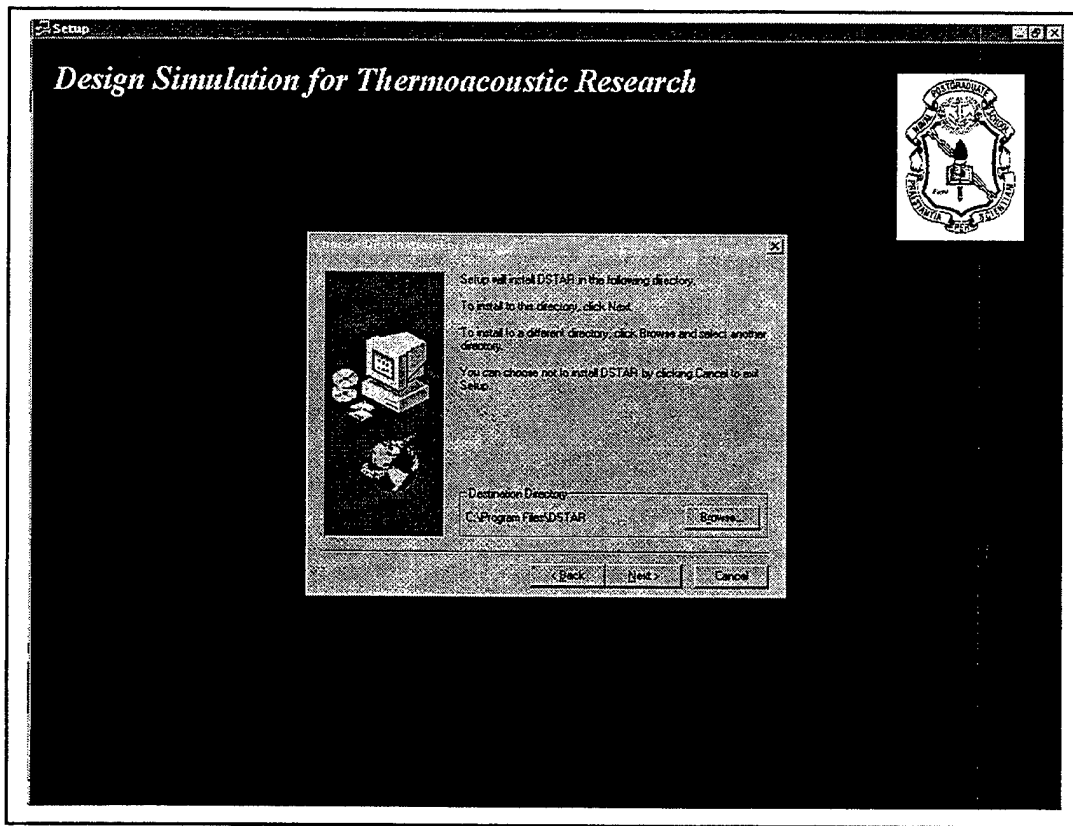, and the results were compared to experimentally gathered values. To verify the thermoacoustic parameters of the modeled device, as determined by DSTAR, the precise and rapid measurement of heat exchanger temperature and acoustic sound pressure level are required.

A.   TEMPERATURE INSTRUMENTS

Temperature is the most important measurable parameter in the operation of a thermoacoustic engine. The temperature of the hot and cold heat exchangers, and the difference between the two, serves to describe at what point the onset and cessation of thermoacoustic effects occur, and directly affects the acoustic power radiated by the device.

In order to measure the temperature of the hot and cold heat exchangers, a **Keithly Instruments**™ Model 740 System Scanning Thermometer was used. The Model 740 allows for the simultaneous measurement of up to 9 thermocouple channels in its standard configuration (one board). For the purposes of performing the measurements

of the thermoacoustic devices, four channels were used; two for the hot heat exchanger, and two for the cold heat exchanger.

The Model 740 allows for the use of a wide variety of thermocouple types, with Type E selected for all measurements contained in this thesis. The Type E thermocouple gives the best response and linearity over the expected range of operation of the thermoacoustic devices analyzed. The most important benefit in using the Model 740 is the ability to utilize the GPIB interface, described in Section C, to read measurements in a rapid fashion from the thermoacoustic device. With all four channels being measured simultaneously, the recorded data allows for a true representation of the instantaneous temperature at multiple points on the device. A detailed description of the operating and measurement characteristics of the Model 740 is provided in Appendix C.

B.   ACOUSTIC INSTRUMENTS

The determination of thermoacoustic onset and cessation, radiated power, and acoustic beam shape, requires a means of precisely measuring the sound pressure level (SPL) at specific points in both time and space. This is accomplished through the use of two **Larson-Davis** ¼" precision microphones. Two microphones are used so that one can be used as a stationary sound pressure level reference, and the second moved to multiple points in the acoustic field to determine radiated beam shape. These microphones are very stable in the acoustic frequency range expected for the analyzed thermoacoustic devices, and provide a very high repeatability of results.

In order to read the output of the **Larson-Davis™** microphones, the output of the microphones are sent to a voltage amplifier that raises the signal to a level easily readable by an attached digital voltmeter. The voltmeter used for the analysis of the devices noted here is a **Hewlett-Packard™ HP 3478A Multimeter**. This multimeter was selected due to its precision over the expected output range of the microphone amplifier (typically in the millivolt range), and its ability to be used with the GPIB interface. The interface allows data to be gathered at a rapid pace, thereby ensuring that all acoustic field data is gathered at the same time as the corresponding temperature data. This allows the accurate determination of acoustic power and thermoacoustic onset and cessation. When used to determine the acoustic field and beam shape, the interface allows for an instantaneous determination of the relative SPL between the two microphones, thereby allowing the determination of the standard 3dB beam shape independent of variations in the overall acoustic field.

In addition to the measurement of the SPL of the acoustic field, the frequency of operation of the thermoacoustic device must be determined. To do this, a **Phillips PM 6669 Universal Frequency Counter** was used. This device enabled the operating frequency to be determined at multiple power levels, including at thermoacoustic onset and cessation. This serves as another parameter that can be compared to the expected theoretical values generated by DSTAR.

C.   GPIB INTERFACE AND CODE

The General Purpose Information Bus (GPIB) interface, sometimes referred to as the proprietary Hewlett Packard Information Bus (HPIB) interface, creates a standard set of commands and protocols through which any compatible instrument can be controlled and monitored from a remote station. The interface allows for the serial or parallel attachment of any number of instruments, each given its own identification code, all responding to instruction issued by the controller, a laptop computer, as shown in Figure 4-1.
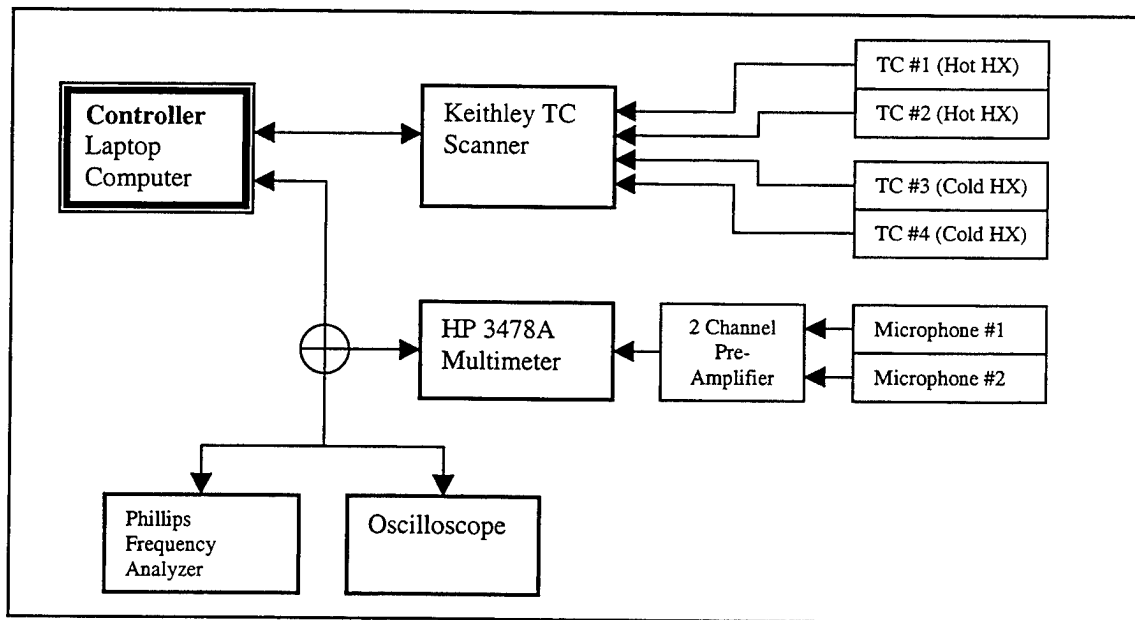
Figure 4-1: GPIB Data Instruments

In order to prepare the instrument and controller assembly for use, the controller must first determine what instruments are attached, and if they are suitable for operation. To do this, the controller issues a command for all attached instruments to respond with

an identification code. The controller then notes and records the identification codes, and will issue all future commands and read measurements based on that specific instrument code.

Once communication between the instruments and the controller has been established, the controller then places all instruments in *remote* mode, where they will only respond to commands from the controller. The instruments are then placed in the required operating modes, as determined by the parameters to be measured. These modes include range, ac/dc volts, temperature scale, thermocouple type, and numerous others. A detailed description of the instrument operating modes used is included in Appendix C.

After the instruments are under the control of the controller, and in the proper operating modes, the controller can record the instantaneous measurement from any device. This is accomplished through the issuing of the *Read()* function, that specifies the instrument to reply as an argument of the function. The instrument will instantly respond with a string containing the measurement information. In this fashion, all instruments can be read simultaneously, and the data recorded, at nearly any data rate desired.

The control of the commands issued by the controller was accomplished through the development of a C++ data gathering program written specifically for the measurements performed, and installed on the laptop. The program utilizes the **National Instruments™ NI-488.2M** library of GPIB class functions to perform all required operations. The program allows for the user to attach multiple instruments, set the desired data recording rate, and writes all data to a user-defined data file for later

analysis. The development of this program was vital to the data measurements, since it allows for the rapid simultaneous measurements of all of the thermoacoustic parameters.

V. MEASUREMENT PROCEDURE

To obtain accurate measurements, it is necessary to minimize thermal and acoustic losses not considered by DSTAR. To accomplish this, it is necessary to measure temperature, SPL, and frequency at as close to steady state as possible. An electrical resistance heater cap, in place of the standard closed end-cap, was used in the experimental analysis of the chosen thermoacoustic device. Further details of this device are provided in Appendix B.

A. DIFFERENTIAL TEMPERATURE VALUES FOR ONSET

Thermoacoustic *onset* is defined as the temperature difference across the stack that results in the radiation of audible sound. During the approach to *onset*, directing acoustic energy into the open end of the resonator tube can stimulate acoustic radiation. However, since the transient acoustic radiation that results will decay, it will not be used as an indication of the point of onset.

To create the required temperature difference across the stack, it is necessary to raise the hot heat exchanger to a very high temperature, while maintaining the cold heat exchanger at a temperature as close to ambient as possible. To accomplish this, the hot heat exchanger temperature was heated by the electrical resistance heater element described in Appendix B. The effects of thermal losses on the experimental results, primarily through free-convection, were evaluated by comparing results, both with and without insulating the hot heat exchanger and end-cap. To maintain the cold heat

exchanger at ambient temperature, convective losses to the atmosphere are relied upon. It was debated whether to apply a heat sink to the cold heat exchanger in the form of a liquid-soaked wrap (i.e. wet rag). However, the application of such a heat sink would create a significant temperature differential within the cold heat exchanger; something that is not accounted for in the DSTAR code. Therefore, it was determined that ambient losses would allow for the most homogeneous temperature throughout the cold heat exchanger, even though some heating would be inevitable. In contrast, during the determination of the radiated acoustic power, repeatability between trials was the overriding factor, and a wet rag was used over the cold heat exchanger and horn to maintain constant temperatures.

The elevation of the temperature of the cold heat exchanger is not relevant to the determination of *onset* over the relatively small temperature range expected, since the *onset* temperature gradient depends mainly upon the temperature ratio between the hot and cold heat exchangers. Any increase in cold heat exchanger temperature would be compensated for by a proportional increase in hot heat exchanger temperature, easily accomplished with the use of the electrical resistance heater.

All experimental measurements were commenced from an ambient condition, with the hot and cold heat exchanger temperatures equal. The electrical resistance heater cap was used to increase the hot heat exchanger temperature in a slow, controlled manner. While temperature was raised, measurements of temperature and SPL were made in expectation of *onset*. As the data in section VII clearly indicates, indications of

54

onset are very clear, and with the slow, controlled temperature rise, the determination of the *onset* temperature is very accurate.

B.   DIFFERENTIAL TEMPERATURE VALUES FOR CESSATION

The determination of the point of *cessation*, where the thermoacoustic device is no longer capable of radiating acoustic energy without outside stimulation, is very similar to the determination of the point of onset. The temperature of the hot heat exchanger was allowed to cool through ambient losses, and the SPL was monitored for an indication of the cessation of acoustic radiation.

A consideration for *cessation* that does not apply to determining the point of thermoacoustic *onset*, is the residual effects of the acoustic field within the device. In the determination of *cessation*, the existing acoustic field can stimulate acoustic radiation even after thermoacoustic *cessation* has occurred. This lag in the loss of acoustic radiation can be reduced through a slow reduction in hot heat exchanger temperature.

C.   SOUND PRESSURE LEVEL AND ACOUSTIC FIELD INTENSITY

To accurately determine the characteristics of the acoustic field radiated by the thermoacoustic device, it is necessary to measure both the magnitude and spatial pattern of the radiated acoustic field. This is accomplished through the use of two high-precision microphones, one a stationary reference and the second a movable. Through the use of two microphones, it is possible to determine the radiation pattern and directivity independent of power variations that may occur due to changes in the temperature profile

across the stack. It is likely that both radiated power and (to a lesser extent) frequency will vary throughout the measurement process, although this was minimized by maintaining the cold heat exchanger at a nearly constant temperature through the use of a wet wrapping around the ambient heat exchanger. By referencing the movable microphone to the stationary one, directivity and directivity index can be determined. Variations in the acoustic frequency are small and while the frequency response of the microphones are very flat, as shown in Appendix C, the directivity of the thermoacoustic device may change very slightly during the measurement.

The symmetrical cross-section of the thermoacoustic devices allows for the assumption of an axi-symmetric radiated acoustic field. To accurately measure the acoustic field, a constant-radius arc of measurement points, as shown in Figure 5-1, was used. The reference microphone was placed on the axis of the device, at a distance of 1 meter, and the second microphone was placed at each of the data points and the corresponding voltages measured. Acoustic field measurements were made in 9 degrees increments.

The microphones were calibrated with a pistonphone providing a stable acoustic source operating at 250 Hz and a SPL of 114.0 dB re 20µPa. The calibration procedure and determination of the appropriate voltage-to-SPL conversion factor is given in Appendix C.
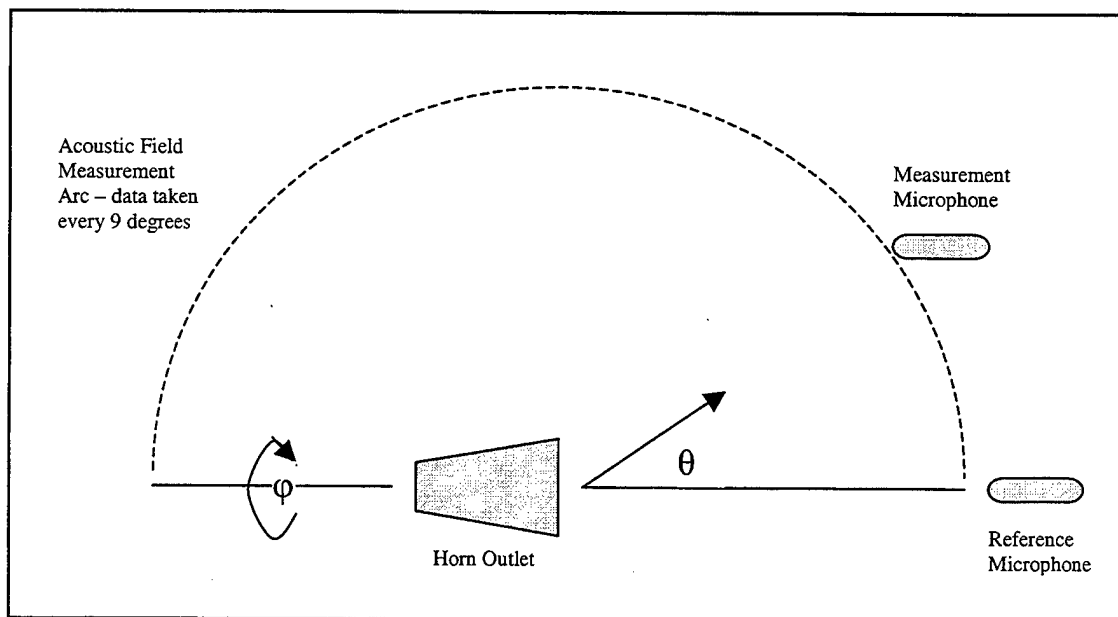
Figure 5-1: Acoustic Field Measurement Grid – Top View

D.   RADIATED POWER

To measure the radiated acoustic power from the open end of the Mini-Hofler

Tube, the radiation pattern must be known, and an appropriate measurement cross-section

selected. While it is possible to model the open end of a horn as a baffled piston for $k \cdot a \gg$

1 [Ref. 9, 12], the small $k \cdot a$ values of the Mini-Hofler Tube, approximately 0.35, preclude

such modeling.

The proper model for the Mini-Hofler tube is to approximate the device as an

unbaffled open-ended resonant tube. Such a tube will have an imperfect impedance

match with the ambient air outside the mouth of the tube that will result in a portion of

the power incident on the mouth being reflected back into the tube. A rigorous

57

examination of this effect is provided by Levine and Schwinger [Ref. 13] with the incident power on the mouth of the tube given by

$$P_{rad} = \pi a^2 |A|^2$$
(5-1)

where A is the residue of the discontinuity of the velocity potential H(ξ) on crossing the surface of the pipe evaluated at $\xi = \pm k$. By applying the reflection coefficient provided by Levine and Schwinger for low-frequency systems (ka < 1),

$$|R| = \exp\left[-\frac{(ka)^2}{2}\right]\left(1 + \frac{1}{6}(ka)^4\left[\log\frac{1}{\gamma ka} + \frac{19}{12}\right]\right)$$
(5-2)

yields the resulting power radiated from the open end of the pipe,

$$P_{rad} = \pi a^2 |A|^2 (1 - |R|^2)$$
(5-3)

Equation 5-3 states simply that the power emitted from the open end of the pipe is the incident power, minus the reflected power, where the amount reflected is based on the efficiency of the impedance matching between the tube outlet and the surrounding air. Typically, impedance matching is accomplished through the use of a flared horn, that has a final radius that yields ka > 3 [Ref. 12]. The development of efficient horns is provided in most acoustics texts, and will not be attempted here. It is important to note, however, that the flared pipe at the termination of the Mini-Hofler Tube does not come anywhere near to meeting the requirements for the impedance matching provided by a horn meeting the classical definition. It is for this reason that the radiation model for an unbaffled tube

developed by Levine and Schwinger, described above, is valid for the Mini-Hofler Tube, as well as most thermoacoustic radiators.

The determination of the acoustic power radiated by the Mini-Hofler Tube can be compared to the power input to determine the thermoacoustic efficiency of the device. These results can be compared with the theoretical efficiency provided by DSTAR. The determination of the total input power uses a thermodynamic power balance approach. The Mini-Hofler Tube is brought to a differential temperature above onset, so that stable acoustic power levels can be maintained. The differential temperature across the stack is maintained constant by the electric heater element providing heat to the hot heat exchanger and by maintaining the cold heat exchanger wrapped in a wet rag that is constantly rewetted with water at room temperature. The total input power to the hot heat exchanger is measured thought the use of a voltmeter and ammeter in line with the electrical power source. The total power balance in steady state is

$$\Pi_{total} = \Pi_{heating} + \Pi_{convection} + \Pi_{radiation} + \Pi_{conduction} + \Pi_{acoustic} \qquad (5\text{-}4)$$

The radiation term is negligible since all high temperature components are shrouded in high-temperature insulation that is a very poor emitter of thermal radiation. Additionally, the convective heat transfer term is also small due to the presence of the insulation. This leaves the terms of *acoustic* and *conduction*. The conductive term is due to the necessary contact between the hot and cold heat exchangers through the stainless steel stack tube, and cannot be reduced without redesigning the device.

The total radiated power is determined by using the intensity measurements described in Section C, above. With the set of measurements made over a 180° arc, the total power incident on a sphere of the radius R is

$$\Pi_{rad} = 2\pi R^2 \int_0^\pi I(\theta)\sin(\theta)d\theta .$$ (5-5)

The efficiency of the device is defined is

$$\eta = \frac{\Pi_{rad}}{\Pi_{total}}$$ (5-6)

VI.   VERIFICATION OF DSTAR PREDICTIONS

A.   THE MINI-HOFLER TUBE

The thermoacoustic device chosen to provide verification of the DSTAR results is
the Mini-Hofler Tube, shown in Figure 6-1. This simple thermoacoustic device provides
a balance between design simplicity and theoretical complexity to fully test the DSTAR
simulation.
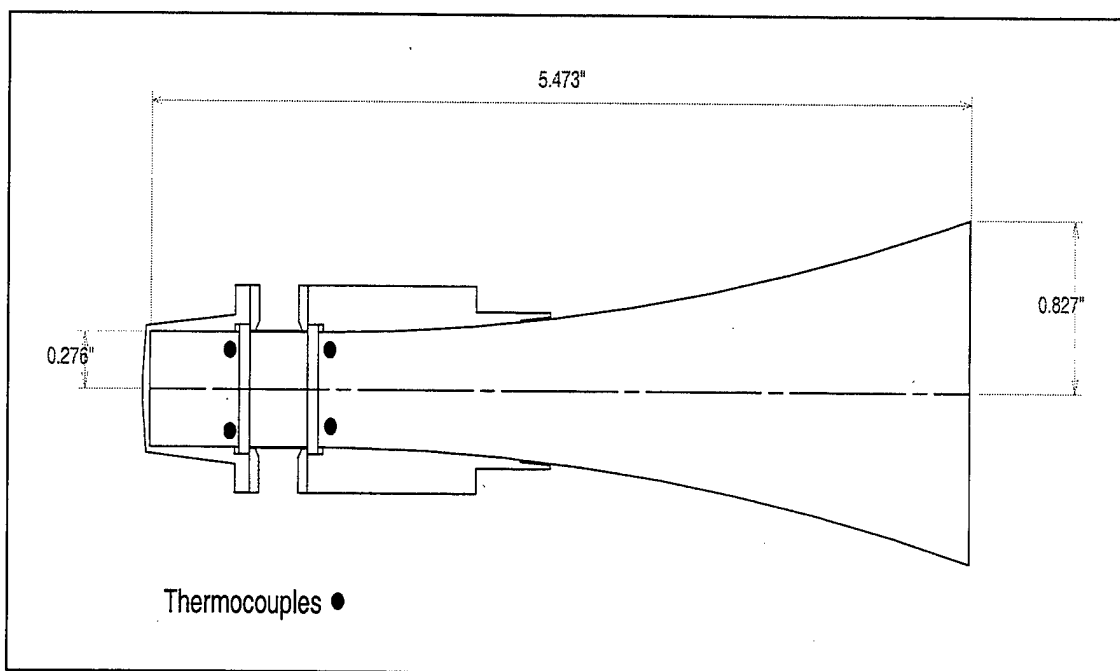
Figure 6-1: The Mini-Hofler Tube Used for Experimental Verification of DSTAR Results

To measure the temperature of the hot and cold heat exchangers, type E
thermocouples were placed as shown in Figure 6-1. Multiple thermocouples provide an
indication of the uniformity of temperature within the heat exchangers.

There are some problems inherent in comparing measured operating parameters
with theoretical DSTAR results for the Mini-Hofler Tube. The first of these is that

losses, primarily in the hot heat exchanger and the stack, are not accounted for in

DSTAR. As part of the experimental verification process, measurements were made to

determine onset and cessation for both a thermally insulated and an uninsulated device.

By measuring the actual thermoacoustic response with and without the effects of

convective heat transfer, it is possible to evaluate the importance of including the effects

of thermal losses in the DSTAR model. The second possible modeling difficulty is the

determination of radiated power. In order to model the acoustic power radiated from the

Mini-Hofler Tube, DSTAR utilizes an approximation in which the tube is modeled as an

open-ended, unflanged pipe. This model does not fully take into account the impedance

matching effects of the flared horn, although these effects are minimal due to the very

high ratio of wavelength to radius at the outlet. Additionally, the Mini-Hofler Tube uses

a carbon RVC stack, which is not properly modeled by DSTAR. This introduces errors

in the boundary values used during the solution of the wave and energy equations, and is

expected to introduce errors in the final results.

B.   ONSET AND CESSATION

The determination of thermoacoustic onset and cessation provides an excellent

comparison of the data generated by DSTAR to measured results. Thermoacoustic onset

is defined as the point at which the device has a sufficient temperature differential

between the hot and cold heat exchangers to cause the device to act as a prime mover and

convert the thermal power to radiated acoustic power. The approximate theoretical point

at which this occurs is given by [Refs. 1,3]

$$\nabla T_{crit} = \frac{T_m \beta \omega p_1^s}{\rho_m c_p \langle u_1^s \rangle}.$$ (6-1)

This indicates that as the mean temperature of the stack increases, primarily due to increases in the cold heat exchanger temperature, the temperature difference required for onset will increase due to the increased mean temperature, and the decreased density of the fluid. In addition, variations in the operating frequency of the device, though small, will have an impact on the temperature of onset.

Since the speed of sound of an ideal gas varies proportional to the square root of temperature, the increased temperature of the air in the device will increase the sound speed, causing an increase in the operating frequency, resulting in an increase in the temperature of onset. All other parameters in Equation 6-1 are relatively independent of temperature over the relatively small range of temperature through which the device operates.

Shown in Figures 6-2 and 6-3 are the results for the uninsulated Mini-Hofler Tube. The upper line is the temperature difference between the hot and cold heat exchangers, and the lower line is the sound pressure level in dB re 20 µPa measured at the outlet of the resonator tube. With constant power is supplied to the electric heater element the temperature rised rapidly and approached a thermal equilibrium state. At approximately 160 seconds into the first run and 815 seconds into the second run, thermoacoustic onset occurs, as indicated by the sudden increase in the sound pressure level from the background level of slightly over 50 dB to approximately 140 dB.
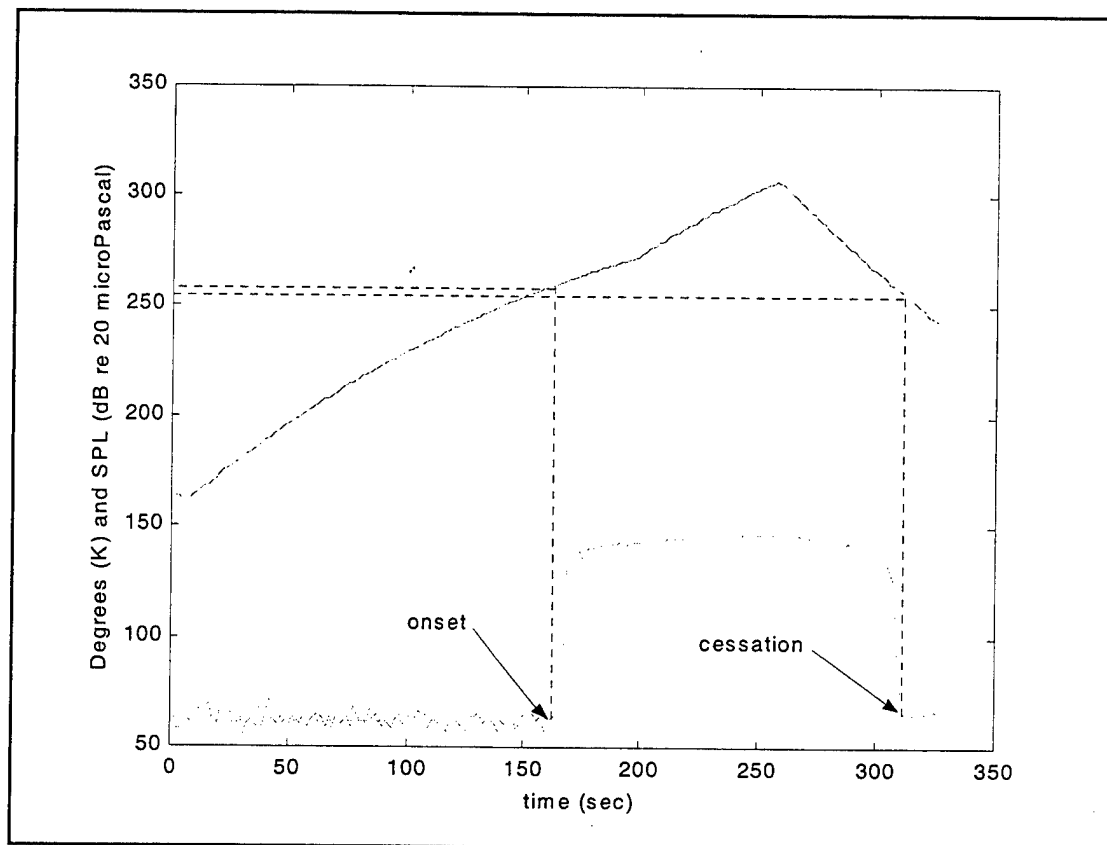
Figure 6-2: Determination of Thermoacoustic Onset and Cessation – Uninsulated

Once thermoacoustic onset occurred, the temperature was allowed to further
increase to determine the effect of stack temperature gradient on radiated acoustic power.
As seen in Figure 6-2, the temperature difference was allowed to increase to a maximum
value of 306.65 K, with a corresponding maximum radiated sound pressure level of 147
dB at the outlet. By comparison, once onset was firmly established, the radiated SPL was
139 dB with a stack temperature difference of 261.9 K.

Figure 6-3: Onset and Cessation at a Constant Stack Temperature Gradient - Uninsulated

Also shown in Figures 6-2 and 6-3 is the occurrence of thermoacoustic cessation.
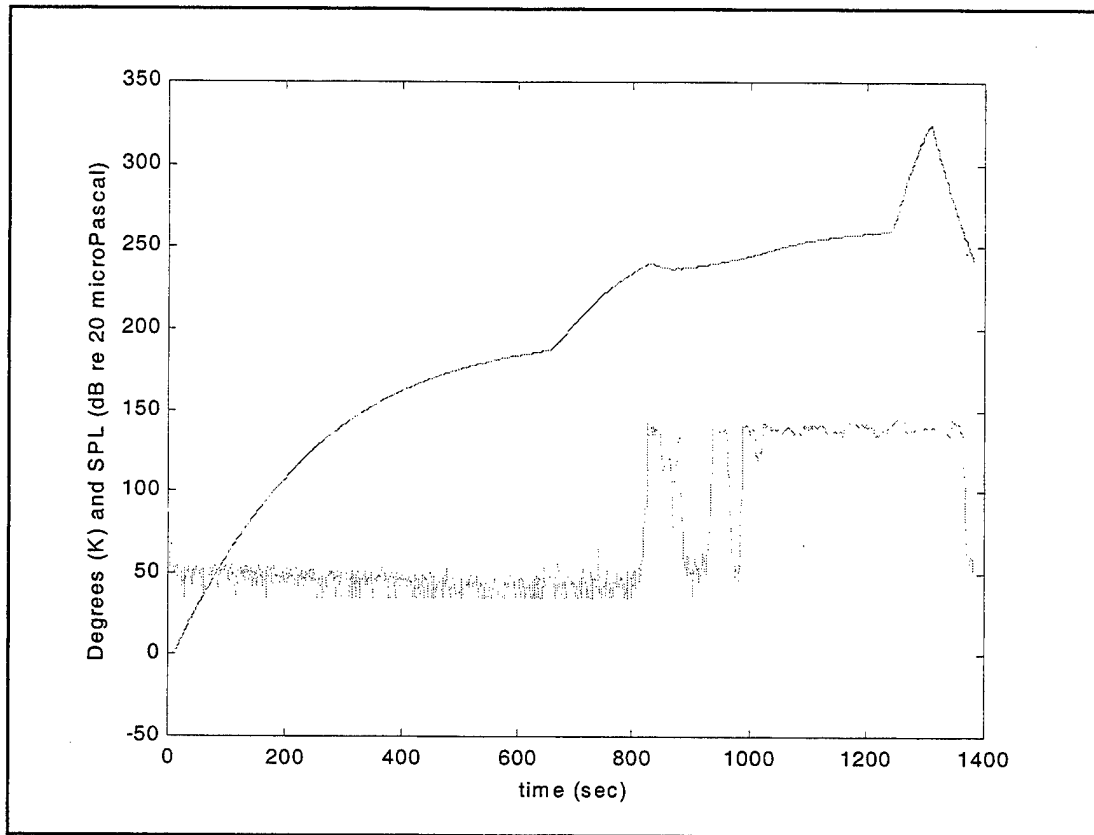
It is noted that in Figure 6-2 the temperature of cessation is slightly lower than that of

onset, meaning that, once established, the condition required to maintain oscillation is

slightly less stringent than those required to initially start the process. This effect is

enhanced further by the fact that the cold heat exchanger temperature is increasing during

the data run requiring an even greater hot heat exchanger temperature to maintain the

oscillations. Figure 6-3 shows this effects in a dramatic way. During this experiment, the

power supplied to the heating element was reduced after onset to study the performance

of the device at that point. As the cold heat exchanger temperature rose due to

65

conduction and thermoacoustic heat transport, the required temperature ratio was no longer met, and cessation occurred. Again, cessation occurred at a differential temperature less than the initial onset temperature difference.

Another set of measurements was made to determine the point of onset and cessation with thermal losses minimized. This was accomplished by heavily insulating the hot heat exchanger and stack. The results of the insulated measurements are shown in Figure 6-4. The results correspond very closely with the results of the uninsulated case in Figure 6-2. This is as expected since a reduction of ambient losses does not affect the determination of the critical temperature difference defined in Equation 6-1. It is important to note, however, that the temperature difference for cessation is now higher than for onset. This is due to the increase in T_m, resulting in a greater temperature differential to maintain operation as a prime mover. The absolute temperature of the hot heat exchanger at onset was 590K, whereas at cessation it was 599K. This increase in temperature of approximately 2% causes a proportional increase in the required temperature difference. With an onset temperature differential of 267K, Equation 6-1 predicts that the critical temperature differential would be 2% higher, or 272K. The observed temperature differential of cessation was 274K, very close to the value predicted by Equation 6-1.

The DSTAR results, as shown in Figure 6-5, are generated from a *tae* file that has the specific design parameters of the Mini-Hofler Tube. All component parameters are identical to that of the device itself, and all global properties are accurate for the environmental conditions existing at the time the data was recorded.
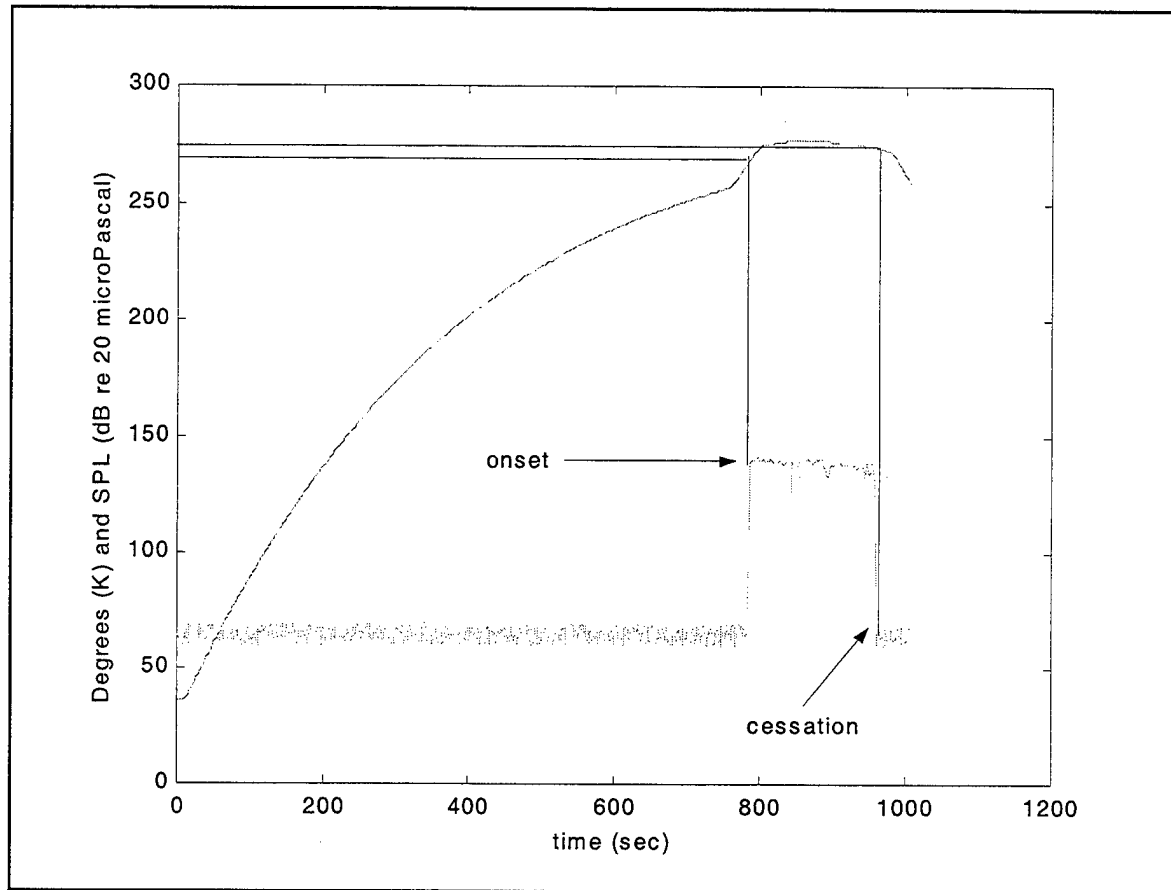
Figure 6-4: Onset and Cessation for an Insulated Mini-Hofler Tube

Shown in Table 6-1 is a comparison of the theoretical parameters as determined by DSTAR with the measured values. The data indicates that DSTAR consistently underestimated the temperatures at which onset occurred by 10-15%, and underestimated the operating frequency for both insulated and uninsulated cases by 3.3%.
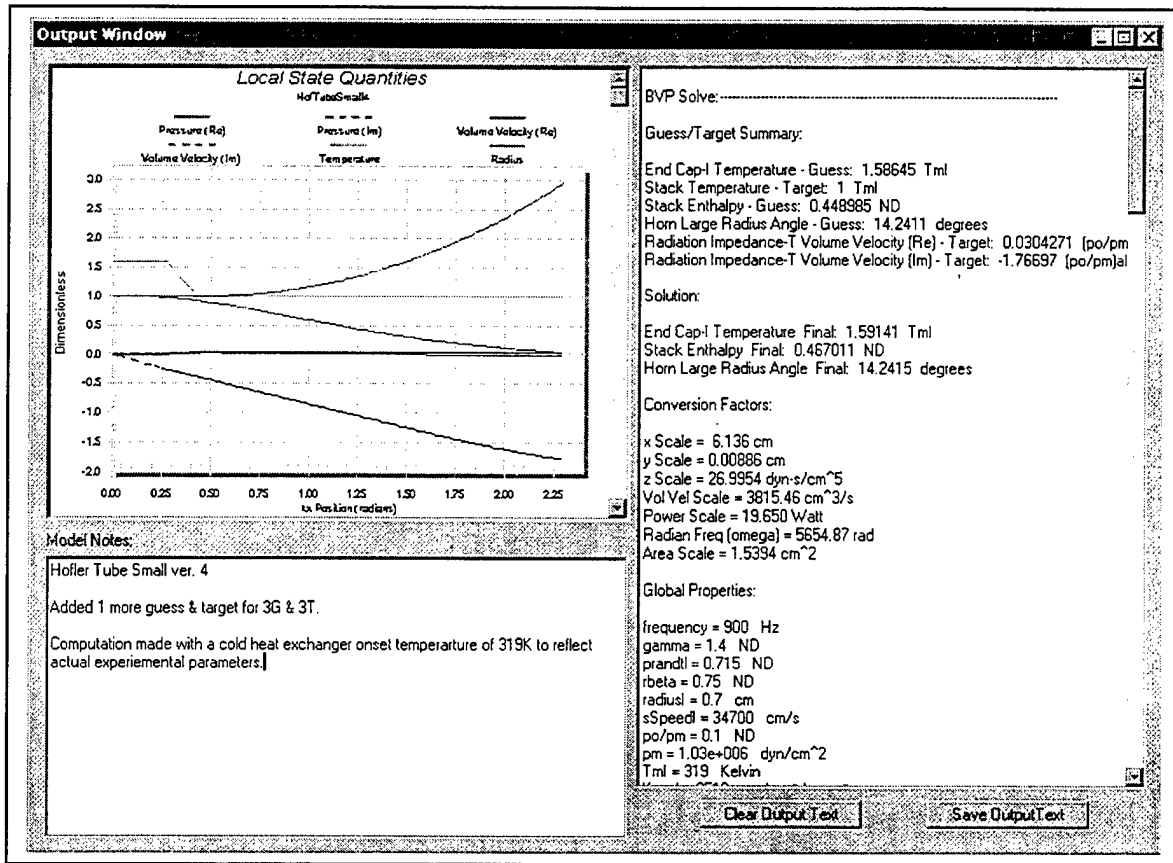
Figure 6-5: Mini-Hofler Tube Operating Parameters as Determined by DSTAR

Parameter Measured	DSTAR Value	Measured Value	Absolute Difference	Relative Difference (%)
Frequency	900 Hz	930 Hz	30 Hz	+3.3%
[1]Onset Hot HX Temp	520.8 K	581.1 K	60.3 K	+10.3%
[1]Onset T_h/T_c	1.62	1.81	0.19	+11.7%
[2]Onset Hot HX Temp	520.8 K	590.7 K	69.9 K	+13.4%
[2]Onset T_h/T_c	1.62	1.83	0.21	+13.0%

[1] uninsulated hot heat exchanger, [2] insulated hot heat exchanger

Table 6-1: Comparison of DSTAR Onset and Frequency Results with Measured Values

68

C.   RADIATED ACOUSTIC FIELD

The spatial geometry of the acoustic field radiated is modeled as an unbaffled tube, which radiates sound in a pattern that depends primarily on the ratio of the wavelength to the radius of the tube, expressed as a k·a value. The smaller the k·a value, the larger the wavelength relative to the diameter of the tube. The k·a of the Mini-Hofler Tube is approximately 0.35, so it is expected to act as a near-omnidirectional source.

A qualitative measure of the amount of directionality of a source is the *Directivity*, D,

$$D = \frac{I_{axial}}{I_{spherical}},$$ (6-2)

where I_{axial} is the intensity on the axis of the tube and $I_{spherical}$ is the intensity at the same point if the source were omnidirectional. Additionally, the directivity is commonly expressed in terms of the *Directivity Index*,

$$DI = 10 Log(D) \text{ dB}.$$ (6-3)

The measured radiation pattern of the Mini-Hofler Tube is shown in Figure 6-6, along with the predicted pattern for a resonant tube with a k·a value of 0.35.

The predicted Directivity of the Mini-Hofler Tube is approximately 1, corresponding to a Directivity Index of 0. The actual observed Directivity of the tube was 1.14 with a Directivity Index of 0.57 dB.
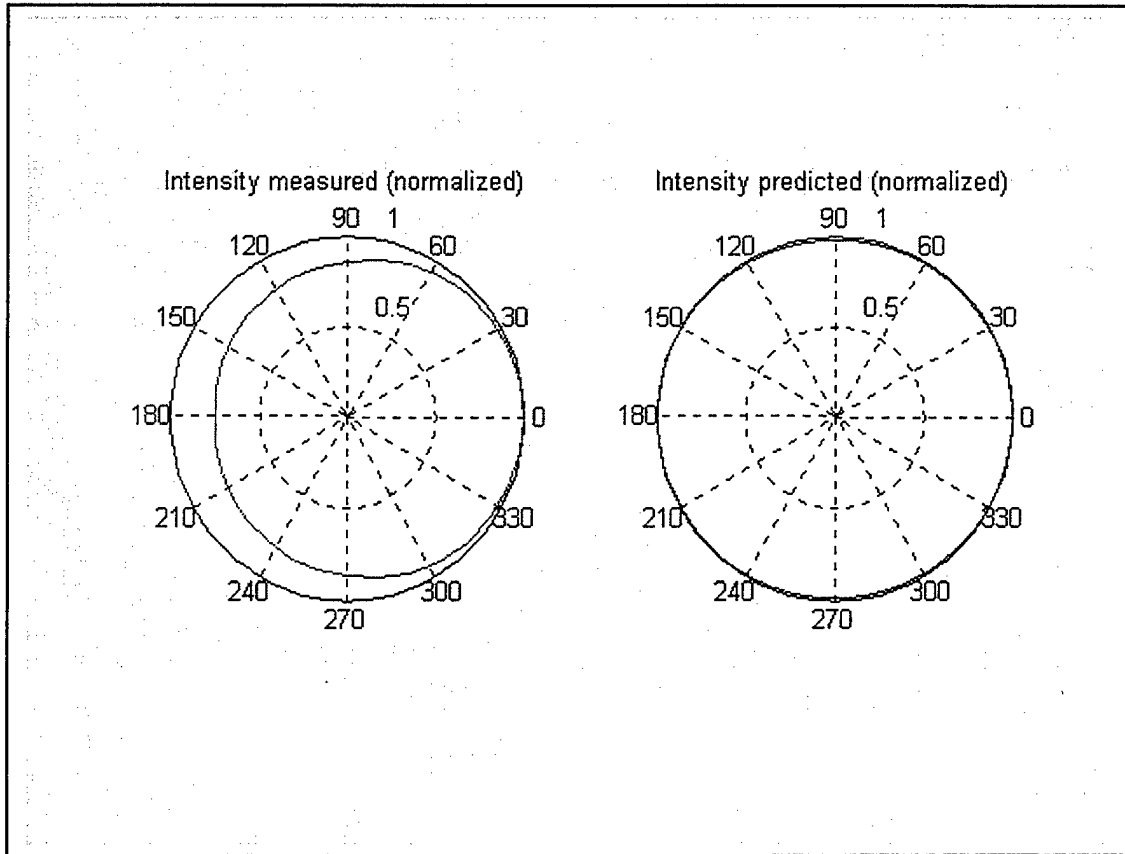
Figure 6-6: Normalized Intensity for Mini-Hofler Tube

D.   RADIATED POWER AND EFFICIENCY

Determining the total radiated acoustic power from the Mini-Hofler Tube

is calculated from the measured acoustic intensity. The total power incident on a sphere

centered around the source is equal to the acoustic power radiated from the Mini-Hofler

Tube.

The radiated acoustic power is 226 ± 40 milliwatts. This compares extremely

well with the DSTAR predicted value of 200 milliwatts, indicating that the viscous and

thermal losses in the resonator are negligible.

Using the procedure for determining the input power, as described in Chapter V, the input power to the Mini-Hofler Tube to generate the acoustic power given above was 13.55 ± 0.04 W.

This input power, when placed into Equation 5-5, along with the total radiated power, yields an acoustic efficiency of 1.67%, compared to the DSTAR prediction of 3.43%. The measured efficiency includes the thermal losses, primarily due to conduction in the stainless steel stack tube, that the DSTAR does not consider. To do a proper comparison of the results, it is necessary to determine the thermal losses from the hot end of the tube, and subtract that amount of power from the total power. The total required power input into the tube is a summation of the power required to raise the temperature of the tube, and the power loss to thermal losses, and is given by

$$\Pi_{input} = \Pi_{\Delta T} + \Pi_{losses} . \tag{6-4}$$

With electrical input power removed, the tube will begin cooling due to thermal losses. The ratio of the heating and cooling rates serves as a proportionality constant, m, between the amount of power required to heat and cool the heat exchanger. Taking the input power to be zero with electrical power secured, the power balance for cooldown is

$$\Pi_{\Delta T} = m\Pi_{losses} . \tag{6-5}$$

Combining Equations 6-4 and 6-5, the power due to thermal losses can be solved for, and this value has been determined to be 5.80 ± 0.06 W.

When this value is subtracted from the total power, the measured efficiency of the Mini-Hofler Tube becomes 2.92 %. This compares well to the DSTAR efficiency of 3.43%. As expected, the measured efficiency is less than the theoretical value, but the

deviation between the two efficiencies, less than 15%, shows that the methodology for determining efficiency used by DSTAR is accurate when thermal losses are taken into account.

VIII. SUMMARY AND RECOMMENDATIONS

A. SUMMARY

The purpose of this thesis was to prepare DSTAR for release as a useful tool in the designing and implementation of thermoacoustic devices. In order to accomplish this, three primary areas had to be addressed; program enhancements and debugging, development of installation and distribution tools, and verification of the accuracy of the code.

The first of these, program enhancements and debugging, included all improvements and corrections to the original DSTAR code developed by Purdy, and additional add-on enhancements. Specific improvements include:

- Improved graphical user interface organization.

- Clarification of terms and output quantities.

- Correction of unit conversion bugs and use of symbology.

- Correction of device geometry scaling errors.

- Implementation of additional commonly-used lumped elements.

- Creation and integration of online Help menus.

- Development of device specific generation of CAD files.

- Implementation of the ability to restore default DSTAR values after changes.

With the changes listed above completed, along with numerous minor usability and convention changes, DSTAR has been improved into a more complete, user-friendly software program that will fulfill the needs of the professional community.

The second area addressed was the development of the ability to distribute the program, along with all required support files. This was accomplished through the development of the installer, as described in Chapter III, and the creation of an internet-accessible web page from which the entire software package may be downloaded. With the downloading of a single self-extracting zipped file, any user may install and run DSTAR with the ease and reliability of any commercially available software package available today.

The final area that this thesis addresses is the accuracy of the DSTAR model in simulating thermoacoustic devices. As described in Chapter VI, DSTAR does an accurate job of simulating the operation of an actual device. The variations noted are most likely due to thermal losses that are unaccounted for within the DSTAR model. Future modifications to the DSTAR code can be made to account for these losses, thereby significantly improving the accuracy of the DSTAR predictions.

B. RECOMMENDATIONS

With the improvements made to DSTAR, and the completion of verification tests that support the accuracy of the existing DSTAR model, it is recommended that DSTAR be made available in the public domain in its present, Version 1.0 form. However,

enhancements to the power and versatility of DSTAR should be made in preparation for the Version 1.x release. Specific improvements include:

- Accounting for thermal losses from the heat exchanger and stack assemblies (e.g. conduction through the stack tube) to more accurately predict thermoacoustically stimulated heat powers.

- The addition of a larger variety of units for user-inputted quantities. This will allow for a more intuitive feel to the magnitude of the input quantities, and the accuracy of the output quantities.

- Perform further verification tests using larger thermoacoustic designs, including designs that have optimum insulation aspects, as would be actually used in real life applications.

Overall, DSTAR has been proven to be an extremely useful tool, but it is clear that it has the potential to be further improved in both power and flexibility. This program is unique in its ability to model an infinite variety of devices, and further improvements should be made to further enhance the strong foundation of the basic DSTAR object model.

APPENDIX A: LIST OF SYMBOLS

a	area	SPL	sound pressure level
c	speed of sound	∇T_{crit}	critical temperature gradient
COP	coefficient of performance	T	temperature (subscript h or c
c_p	isobaric heat capacity per unit		indicates hot or cold reservoir)
	mass	T_∞	bulk fluid temperature
D	diameter	T_m	mean temperature
f	frequency	W	work
g	gravity ($9.81 \ m/s^2$)	$\dot{W}$	work flow
H,h	enthalpy	y_0	plate half-gap
$\dot{H}$	total enthalpy flow	α	thermal diffusivity
$H(\theta)$	directional factor	β	thermal expansion coefficient
i	imaginary number	γ	ratio of specific heats
I	initial or intensity	δ_k	thermal penetration depth
Im	imaginary part	δ_v	viscous penetration depth
k	wave number	η_c	Carnot efficiency
K	thermal conductivity	η	efficiency
l	plate half-thickness	ε_s	plate heat capacity ratio
L	length	κ	thermal diffusivity or elasticity
ND	non-dimensional	λ	wavelength
P,p	pressure	μ	dynamic viscosity
Pr	Prandtl number	υ	kinematic viscosity
Q	thermal energy (subscript h or c	Π	power
	indicates hot or cold reservoir)	ρ	density
$\dot{Q}$	thermal energy flow	σ	Prandtl number
r	radius	ω	angular frequency
Re	real part		

Normalized Variables and Parameters:

P	$= p_1/p_o$	dynamic pressure variable
U	$= U_1/N_U$	volume velocity variable
T	$= T_m/T_{mI}$	mean temperature variable
X	$= k_I x$	x position variable
R	$= r_w/r_{wI}$	inner radius variable or parameter
Y	$= y_o/\delta\kappa_I$	stack plate gap parameter
L	$= l/y_o$	stack plate thickness parameter
H$_2$	$= H_2(1+L)(r_{wI}/r_{st})^2/N_P$	stack enthalpy parameter (r_{st} is stack radius)
K	$= (K+LK_s)k_I T_{mI}/N_{PD}$	longitudinal thermal conduction parameter in stack
W$_2$	$= Re(\mathbf{P}\tilde{\mathbf{U}})$	acoustic work power; Not normalized is $W_2 = N_P Re(\mathbf{P}\tilde{\mathbf{U}})$

APPENDIX B: MINI-HOFLER TUBE SPECIFICATIONS

Hot Straight Tube:
    $L = 1.59$ cm
    $r = 1.43$ cm

Hot Heat Exchanger:
    $L = 0.19$ cm
    $r = 1.43$ cm
    $y_0 = 0.043$ cm
    $l = 2.8e\text{-}5$ cm

Stack:
    $L = 1.02$ cm
    $r = 1.43$ cm
    $y_0 = 0.032$ cm
    $l = 2.8e\text{-}6$ cm

Ambient Heat Exchanger:
    $L = 0.19$ cm
    $r = 1.43$ cm
    $y_0 = 0.043$ cm
    $l = 2.8e\text{-}5$ cm

Resonator Tube:
    $L = 11.61$ cm
    $r_i = 1.43$ cm
    $r_f = 4.29$ cm
    $\theta_i = 0$ deg
    $\theta_f = 14.24$ deg

Mounted on the endcap of the Mini-Hofler Tube are two electrical resistance heaters embedded within a block of iron (shown in Figure B-2). This provides a stable and variable heat source that is relatively free of fluctuations in temperature, due to the large heat capacity of the block.
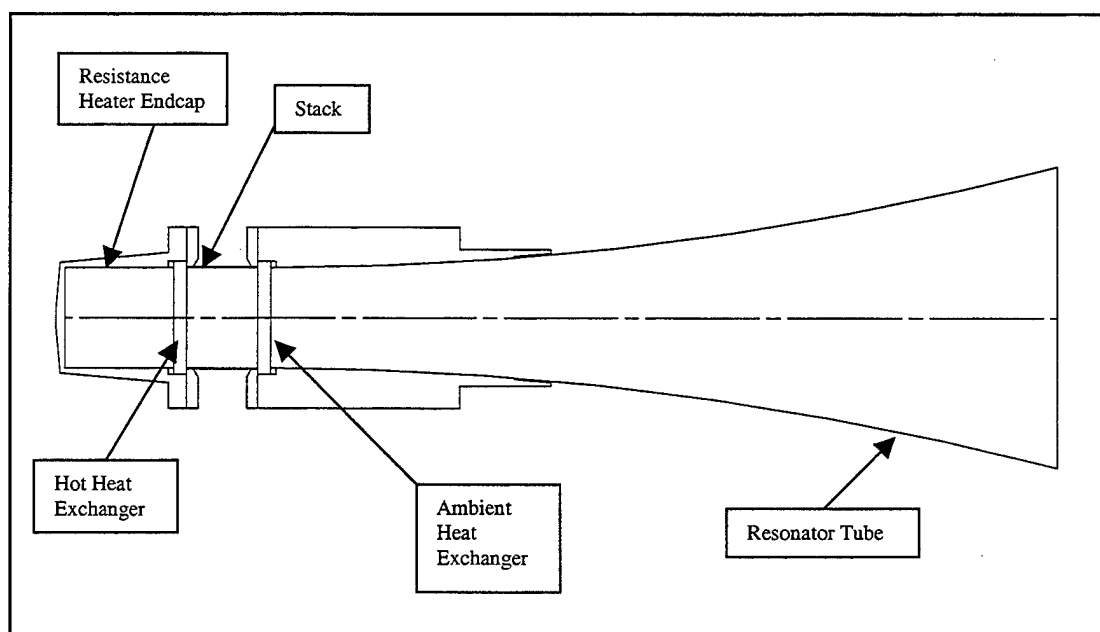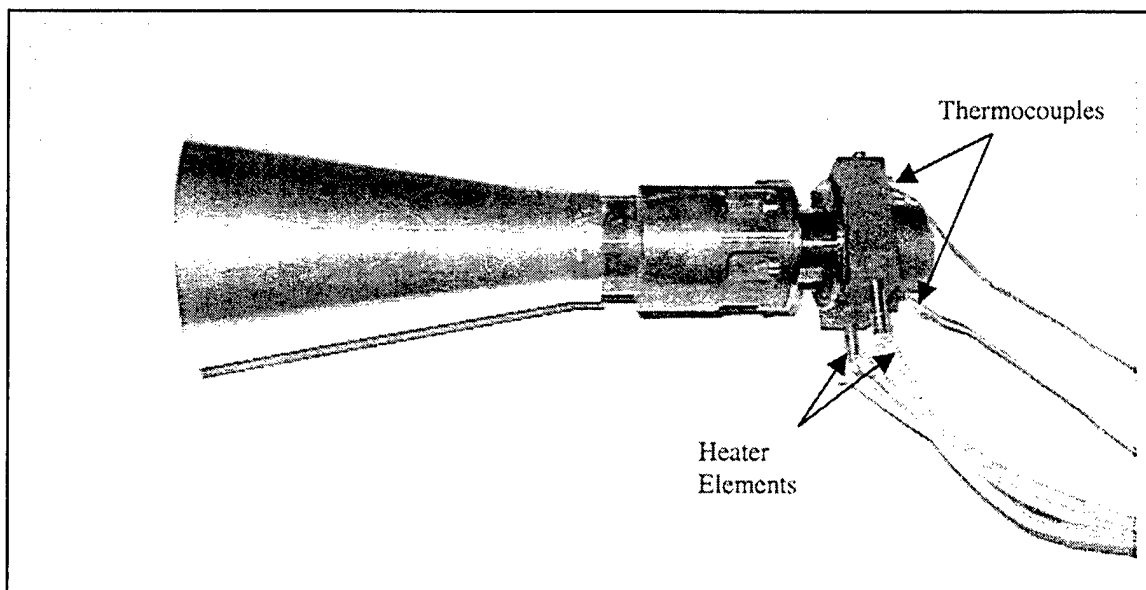

Figure B-1: Mini-Hofler Tube

Figure B-2: Mini-Hofler Tube with Electric Heater and Hot Thermocouples Shown

APPENDIX C: MEASUREMENT DEVICE SPECIFICATIONS

Keithley Instruments Model 740 System Scanning Thermometer

s/n 496518
calibrated 3-19-1991
range (type E TC) –100°C - 1000°C
accuracy ± 0.5°C

Mode used for data:
Scale:	Celcius (O0)*	
Filter:	on (P0)	
Display:	Temperature (D0)	
Triggers:	Continuous (T0)	
Function:	Current Channel (F0)	
Read Mode:	Current Channel (B0)	
Data Format:	Single Output (G3)	

All measurements were conducted with at an ambient temperature of 20.1°C.

Hewlett-Packard HP3478A Multimeter

s/n 2911A59877
range 0-300 mV
resolution 1 μV
accuracy ± 0.1%

Mode used for data:
Scale:	300 mV DC (R-2)	
Display:	5 ½ digit display (N5)	
Trigger:	Internal Trigger (T1)	
Autozero:	On (Z1)	

Phillips PM 6669 Universal Frequency Counter

range 0-10000 Hz
resolution 0.01 Hz
accuracy ± 3 Hz (estimated due to reading fluctuations)

---

* Codes in parenthesis represent GPIB standard interface codes.

Larson-Davis Model 2530 ¼" Microphone

s/n 1207
sensitivity   −56.6 dB re 1V/Pa
                1.48 mV/Pa
calibration data
                8.40e-3 volts with gain = 10, bias = 100 volts
                2.34e-3 volts with gain = 0, bias = 100 volts

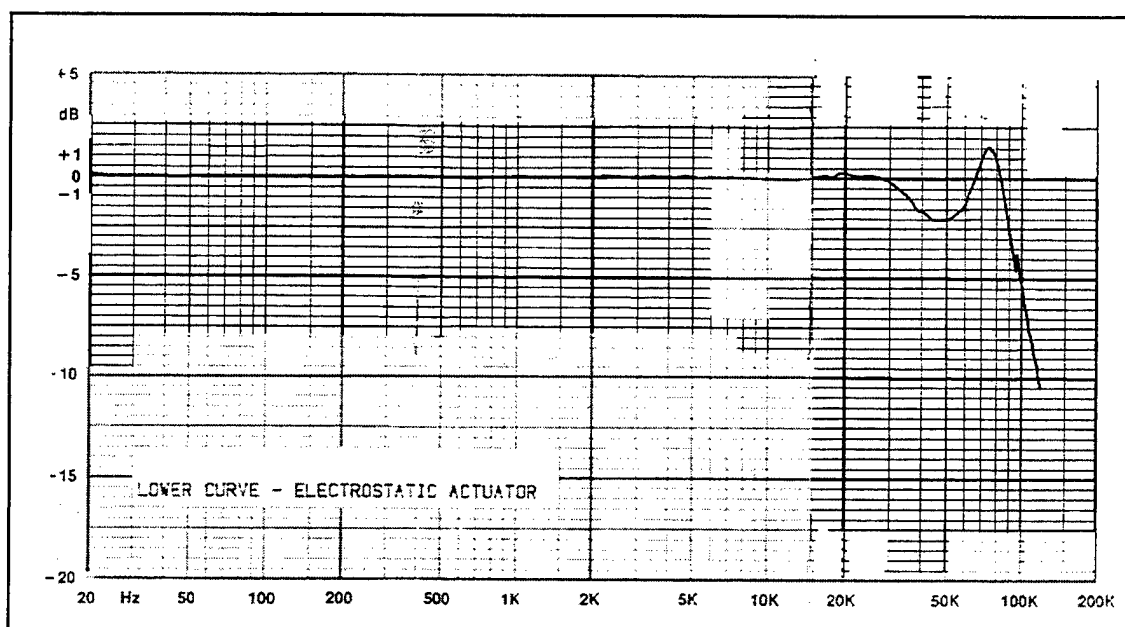Frequency response shown in Figure C-1

Figure C-1: Microphone Frequency Response

Microphone Calibration

Using this piston-phone calibration device, and measuring the corresponding

voltage output of the microphones, a conversion factor from output voltage to acoustic

intensity within the far-field is obtained by using the equivalent reference of 10^{-12} W/m^2 ~

20μPa [Ref. 9]. This factor is defined by

$$10\log(\frac{I}{10^{-12}W/m^2}) = SPL(dB).$$ (C-1)

Solving for intensity, I, in W/m^2 yields

$$I = \log^{-1}(\frac{dB}{10}) * 10^{-12}W/m^2,$$ (C-2)

which is then transformed into a linear voltage conversion factor according to

$$I = 29.9\frac{W/m^2}{Volt}.$$ (C-3)

LIST OF REFERENCES

1. Swift, G.W., "Thermoacoustic Engines and Refrigerators", *Physics Today,* pp. 22-28, July 1995.

2. Purdy, E.W., "Development of a Graphical Numerical Simulation for Thermoacoustic Research", December 1998.

3. Wheatley, J.C., Swift, G.W., and Migliori, A., "The Natural Heat Engine", *Los Alamos Science,* number 14, pp. 2-29, Fall 1996.

4. Moran, M.J., Shapiro, H.N., *Fundamentals of Engineering Thermodynamics,* John Wiley and Sons, 1988.

5. Swift, G.W., "Thermoacoustic Engines", *Journal of the Acoustical Society of America,* v.84, p. 1145-1179, 1988.

6. Wong, K., "Solving Ordinary Differential Equations with Runge-Kutta Methods", June 1996, [www.geog.ubc,ca/numeric/labs/lab4/lab4/lab4.html].

7. Kreyszig, E, *Advanced Engineering Mathematics,* 6th ed, John Wiley and Sons, 1988.

8. Allen, R.C., Avery, P., and Wallace, J.Y., "Lower/Upper Triangular (LU) Decomposition", *Computational Science Textbook,* Sandia Corporation, 1998, [ais.cs.sandia.gov/AiS/textbook/textbook.html].

9. Kinsler, J.W., Frey, A.R., Coppens, A.B., and Sanders, J.V., *Fundamentals of Acoustics,* 3rd ed., John Wiley and Sons, 1982.

10. Morse, P.M., Ingard, K.U., *Theoretical Acoustics,* Princeton University Press, 1968.

11. Incropera, F.P., DeWitt, D.P., *Fundamentals of Heat and Mass Transfer,* 3rd ed, John Wiley and Sons, 1990.

12. Pierce, A.D., *Acoustics: An Introduction to its Physical Principles and Applications,* McGraw Hill, 1981.

13. Levine, H., Schwinger, J., "On the Radiation of Sound from an Unflanged Circular Pipe", *Physical Review*, Volume 73, Number 4, February 1948.

INITIAL DISTRIBUTION LIST

No. of copies

1. Defense Technical Information Center 2
    8725 John J. Kingman Rd., STE 0944
    Ft. Belvoir, VA 22060-6218

2. Dudley Knox Library 2
    Naval Postgraduate School
    411 Dyer Rd.
    Monterey, CA 93943-5101

3. Professor Thomas J. Hofler, Code PH/Hf 4
    Naval Postgraduate School
    Monterey, CA 93943-5100

4. LT Scott B. Curtis 2
    10907 165th Place NE
    Redmond, WA
    98052